J. Appl. Comput. Mech., 8(3) (2022) 809-830
DOI: 10.22055/JACM.2020.32443.2015

ISSN: 2383-4536
jacm.scu.ac.ir

Shahid Chamran University of Ahvaz

Journal of Applied and Computational Mechanics

Research Paper

# Optimization of Air Distribution Patterns by Arrangements of Air Inlets and Outlets: Case Study of an Operating Room

Vahid Gholami Motlagh[1], Mohammad Ahmadzadehtalatapeh[2]

[1] Department of Mechanical & Marine Engineering, Chabahar Maritime University, Chabahar, 99717-56499, Iran, Email: v_gholami@yahoo.com

[2] Department of Mechanical & Marine Engineering, Chabahar Maritime University, Chabahar, 99717-56499, Iran, Email: m.ahmadzadeh@cmu.ac.ir

Received January 30 2020; Revised May 09 2020; Accepted for publication May 15 2020.
Corresponding author: M. Ahmadzadehtalatapeh (m_ahmadzadeh56@yahoo.com; m.ahmadzadeh@cmu.ac.ir)


**Abstract.** In this research, possible methods to improve the air distribution patterns of an operating room (OR) employing CFD method are investigated. Laminar airflow (LAF), turbulent airflow (TAF), and LAF with the air curtain are examined. It is found that LAF and LAF with the air curtain cases are superior to TAF-based cases. The study shows that the LAF and LAF with the air curtain cases as the proposed configurations have an acceptable capability to maintain the indoor air conditions within the range recommended by the standards. According to the simulations, the LAF with the air curtain case is the most suitable case in terms of the contamination risk, and it is recommended to be implemented in the existing OR.

**Keywords:** Air distribution patterns, Airflow, CFD method, Operating room (OR).

## 1. Introduction

Hospitals, medical centers, and operating rooms (ORs), as clean spaces, require sophisticated heating, ventilation and air conditioning (HVAC) systems in order to provide a comfortable environment for the occupants and pollutions need to be controlled to minimize the risk of surgical infections [1,2]. Pollution in the ORs is normally being produced by dust, occupants' breath, bacteria from people's bodies, and medical instruments, as well as the circulation of anesthetic gases [3-5]. Moreover, the primary transport mechanism for the bacteria in the ORs is the skin flakes or squames release from the exposed regions of the surgical staff and patient. Such squames are approximately 25 microns (μm) in diameter and 3 to 5 microns in thickness. During a typical two-hour surgery, about 1.15 to 90 million squames are estimated to be released into the ORs space [6]. As mentioned above, the gases emitted from the patient and personnel's breathing are among the sources of pollution in the ORs. The exhalation of the patient and personnel causes the production of $CO_2$ and increases its concentration in the ORs. The relevant standards recommend the concentration level of $CO_2$ to be less than 1500 ppm in the ORs [7].

ORs need unique requirements in order to provide clean and desirable indoor air conditions [8]. A standard design of HVAC systems is essential to provide comfortable and healthy indoor air conditions for the occupants of an OR, including patients, doctors, and nurses. A non-standard HVAC system in an OR can also affect the effectiveness of the surgical team functioning procedures [8]. Different standards and guidelines have been introduced for ORs. Table 1 presents the different standards and guidelines suggested for the ORs design [9].

Every year, about four million hospital infections occur, leading to 20 to 80 thousand deaths in the world [5]. Therefore, air distribution in the ORs is an essential factor leading to protecting the patients and the surgical team against infections and establishing comfort for the occupants [9-11].

**Table 1.** HVAC guidelines for ORs [9].

| Standards and guidelines | Room air temperature $T_r$ (°C) | Supply air temperature $T_a$ (°C) | RH (%) | Supply air velocity (m/s) |
|---|---|---|---|---|
| DIN 1946 | 19-26 | $T_a<T_r$ | a | $\upsilon \geq 0.23$ |
| VDI 2167 | 22 | $T_a<T_r$ | 30-50 | $\upsilon \geq 0.23$ |
| ASHRAE 170 (2008) | 20-24 | a | 30-60 | 0.13-0.18 |
| ASHRAE application handbook | 17-27 | a | 45-55 | 1.3-1.8 |

[a]Value not specified.

Published online: May 15 2020

Different ventilation systems are applied in the ORs. The turbulent airflow (TAF) method is one of the systems in which the air enters into the OR through the diffusers installed in the roof (ceiling air supply) or at the walls. In this system, the turbulence occurs in the airflow direction, while the air enters into space. Due to this phenomenon, this system does not have proper control over the airflow and air distribution patterns in the OR. The laminar airflow (LAF) method is another system employed in the ORs. In this method, the air is supplied in a horizontal or vertical direction. However, the vertical supply has advantages over the horizontal system. In the vertical system, the suspended particles moves downward by the airflow, and pollutants are being reduced. In the LAF system with the air curtain, as LAF system, uniform flow is supplied from the diffusers on the four sides of the surgical bed, and due to the high velocity of the exhaust air from the diffusers, the air acts as a barrier around the area [12].

The literature review indicates that there are valuable experimental and numerical studies on the airflow distribution, thermal comfort, and various factors leading to the infection in ORs [8-30]. For instance, McNeill et al. [8] investigated the air distribution in an orthopedic surgery room. For this purpose, the surgeons, nurses, anesthetist, and patient were substituted by five manikins, and flow visualization techniques with particle image velocimetry (PIV) were utilized. Ufat et al. [10] analyzed the three-dimensional air distribution of ORs with different velocities and temperatures with different exhausts. In this study, two models were considered, and the velocity, temperature, and relative humidity (RH) distribution were explored. It was shown that temperature and RH in the designed models had no significant variation. It was also observed that the inlet air velocity in the installed exhausts in two corners was increased; therefore, it prevented a proper air distribution around the surgical bed. However, it was shown that the air distribution for the system with the exhaust from the four corners was more regular than the examined models and the risk of infection in the system was lower than other studied models. In another study, Zhai and Osborne [11] studied the feasibility of improving ventilation systems for the ORs. The results showed that unidirectional flow provided by LAF diffusers is a reliable method for maximizing the air disinfection by the use of high-velocity air curtains.

The risk of contaminant deposition in an OR was investigated by the airflow modeling and particle tracking methodologies by Memarzadeh and Manning [13]. It was reported that ventilation systems that provide laminar flow conditions are the best choice, and a face velocity of about 0.15m/s to 0.18m/s is sufficient from the laminar diffuser arrays. Using the computational fluid dynamics (CFD) method, Memarzadeh and Jiang [6] studied the effect of OR geometry and variations of HVAC system parameters on the protection of the surgical site. It was shown that LAF arrays should cover heat release sources such as the surgical team and surgical lights. In another study, Chow and Yang [14, 15] discussed the basic principles of the ORs. To this end, seven different cases with different situations for the surgical lights and different supply air velocities were studied using CFD method. The health risks caused by the airborne bacteria released from the surgery personnel and the patient were emphasized in the study. In another research, Chow et al. [16] investigated the effect of surgical lights location and the supply air velocity in ultra-clean ventilation in an OR. It was declared that changes in the velocity of supply air and the position of the surgical lights do not have a significant effect on the occupants' thermal comfort. An overview of the design principles of indoor thermal conditions in ORs was presented by Balaras et al. [17]. Rui et al. [18] explored the strategy of bacterial contaminant controlling in an OR with different ventilation models. In this study, a numerical simulation to determine the path of the particles was also conducted. It was shown that the flow pattern improvement could decrease the particle's deposit on the critical surfaces. However, this impact would be less evident when the air change rate increases to a certain amount. It was also found that with the rise of air velocity beyond a certain value, the particle's deposit was increased.

Ho et al. [19] performed a three-dimensional CFD analysis for the thermal comfort and contaminants removal from an OR. The effect of supply air and exhaust positions on the thermal comfort and contaminant removal were investigated. Horizontal airflow for airborne particle control in ORs was investigated by Liu et al. [20]. In this study, an experimental and CFD simulation study were employed. El Gharbi et al. [21] conducted a study on the analysis of indoor air quality for ORs using experimental measurements and numerical modeling techniques to determine the RH and temperature distribution. Different supply and exhaust air locations were examined, and it was recommended that an appropriate method for sterilizing the operating area is unidirectional air supply. Yau and Ding [22] investigated the air distribution of an OR in the Sarawak General Hospital heart center in Malaysia. In this study, the effect of surgical lights on air distribution was examined. The study revealed that the location and situation of the surgical lights could affect the airflow profile such that air with a high velocity around surgical lights might cause an air barrier around these lights leading to an improper air distribution beneath the surgical lights. The temperature distribution, contaminant concentration, humidity, and velocity distribution in two systems with even and uneven airflow situations were also investigated in the study. The decrease in inlet flow rate of about 15% for energy saving was recommended in the study. A computing model for predicting the vertical temperature in the ventilation system of impinging jet ventilation (IJV) was developed by Kobayashi et al. [23]. In this study, a parametric investigation on the supply air velocity and its effect on the thermal layer is conducted.

The literature survey indicates that there is extensive research on the HVAC system's performance in the ORs. To the authors' best knowledge, no previous comparative study has been reported numerically to investigate the performance behavior of TAF (Cases 1 to 4), LAF (Cases 5 and 6), and LAF with the air curtain system (Case 7) in an OR. Therefore, this research was conducted, and the major aim was to explore the possibility of improving the air distribution in an OR by examining different cases in terms of inlet and outlet layouts to recommend the most appropriate case for the patient and the surgical team.

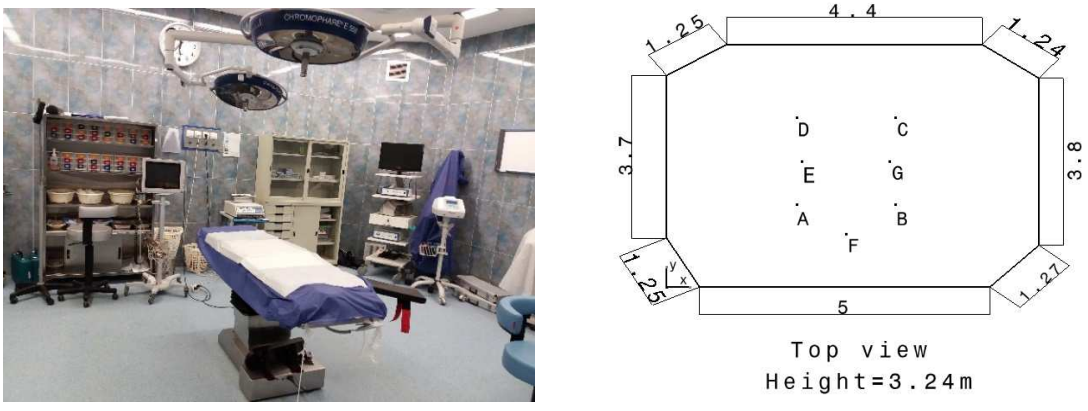


(a) (b)

**Fig. 1.** The OR overview: (a) interior view and (b) dimensions (in meters).

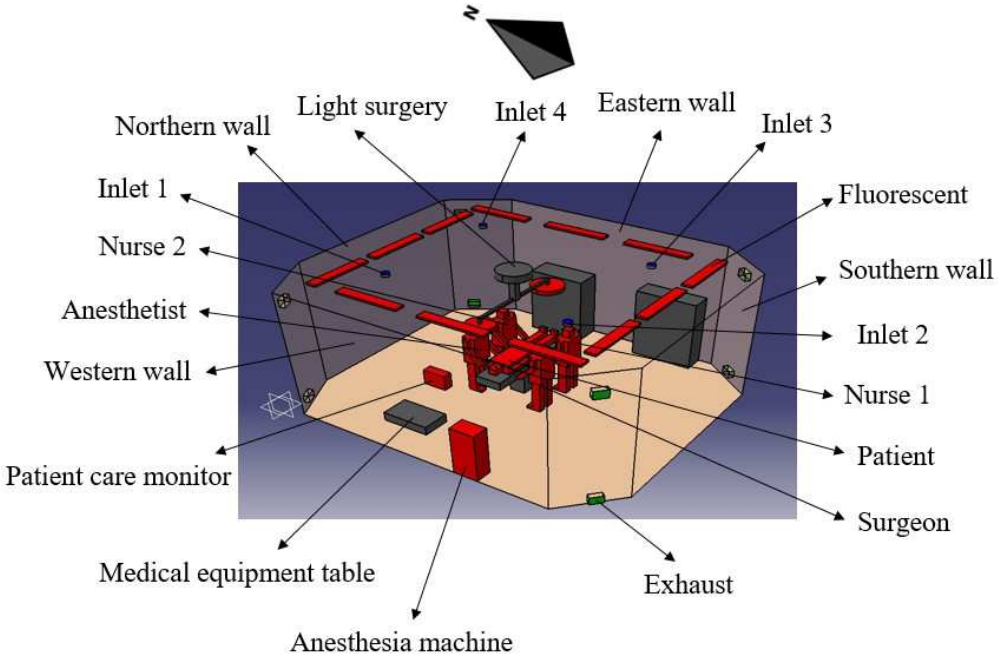


**Fig. 2.** The layout of the simulated OR (Case 1).

## 2. Research Methodology

In this section, the research methodology is presented. The geometry of the existing model and the examined cases are described in Subsection 2.1 first. Then, the governing equations and the simulation process will be explained in Subsections 2.2 and 2.3-2.7, respectively.

### 2.1 Model geometry

In the present research, an OR in the Iranian Surgery Clinic (ISC), Chabahar, Iran, was considered for the investigation. This clinic is located in Chabahar Free Zone, Iran. Fig. 1 shows the interior view of the considered OR and its dimensions. The simulation validation points (A, B, C, and D) and the mesh independence axes (E, F, and G) are also illustrated in Fig. 1.

Fig. 2 shows the isometric view of the OR (existing condition, Case 1). The ventilation system employed in the OR is the TAF method, and the instruments, diffusers, and the operating table are illustrated in Fig. 2. In Fig. 2, the two gray blocks beside the eastern wall show the wardrobes, and the gray block beside the western wall represents the equipment table. Anesthesia machine and patient care monitor as the heat sources are shown with two red blocks. The OR has four inlets with a circular section (blue surfaces) on the ceiling and eight outlets with a rectangular section (green surfaces) in the chamfered corners. Size and dimensions of the inlet diffusers, outlet vents, and other equipment in the OR, including surgical bed, ceiling lights, and surgical lights, are tabulated in Table 2.

**Table 2.** Nomenclature and dimensions for Fig. 2.

| Item | Quantity | Dimension (m) |
|---|---|---|
| Surgical bed | 1 | 0.5 × 1.98 × 0.2 |
| The basis of the surgical bed | 1 | 0.305 × 0.35 × 0.68 |
| Anesthesia machine | 1 | 0.46 × 0.315 × 1.22 |
| Surgical light 1 | 1 | 0.6 diameter × 0.1 |
| Surgical light 2 | 1 | 0.51 diameter × 0.1 |
| Human model | 5 | 1.7 height |
| Mouth | 5 | 0.04 × 0.02 |
| Patient care monitor | 1 | 0.42 × 0.17 × 0.36 |
| Medical equipment table | 1 | 0.83 × 0.49 × 0.2 |
| Each pair of lamps | 12 | 1.2 × 0.19 × 0.05 |
| Medical equipment wardrobe | 1 | 1.18 × 0.4 × 1.81 |
| Medicine wardrobe | 1 | 1.1 × 0.5 × 1.7 |
| Inlet diffuser | 4 | 0.146 diameter |
| Outlet vent | 8 | 0.235 × 0.185 |
| OR (all the cases) | 7 | Fig. 1: (b) |

**Table 3.** Dimensions and the quantity of inlet diffusers and outlet vents.

| Case number | | | Quantity | Dimension (m) | Total areas (m²) | ACH |
|---|---|---|---|---|---|---|
| Case 1 | | Inlet | 4 | 0.146 diameter | 0.0669 | 5.87 |
| | | Outlet | 8 | 0.235 × 0.185 | 0.3478 | |
| Case 2 | | Inlet | 4 | 0.27 diameter | 0.2289 | 20 |
| | | Outlet | 4 | 0.235 × 0.185 | 0.1739 | |
| Case 3 | | Inlet | 4 | 0.27 diameter | 0.2289 | 20 |
| | | Outlet | 4 | 0.235 × 0.185 | 0.1739 | |
| Case 4 | | Inlet | 4 | 0.27 diameter | 0.2289 | 20 |
| | | Outlet | 4 | 0.235 × 0.185 | 0.1739 | |
| Case 5 | | Inlet | 4 | 0.62 × 1.2 | 2.976 | 20 |
| | | Outlet | 8 | 0.235 × 0.185 | 0.3478 | |
| Case 6 | | Inlet | 4 | 1.2 × 0.62 | 2.976 | 20 |
| | | Outlet | 8 | 0.235 × 0.185 | 0.3478 | |
| Case 7 | Inlet | Main Diffuser | 1 | 1.11 × 2.59 | 2.8749 | 31.6 |
| | | Air Curtain | 1 | - | 0.502 | |
| | | Outlet | 8 | 0.235 × 0.185 | 0.3478 | |

Various configurations for the inlet and outlet layouts were studied as the different cases, namely Case 1 to Case 7, to examine the possible improvements in the air distribution and indoor air conditions in order to recommend the most desired layout for the considered OR. Dimensions and the quantity of the inlet diffusers and outlet vents for the cases are tabulated in Table 3. The air change per hour (ACH) as the ratio of the total volume of incoming air to the total space volume [3, 24] was determined from the fieldwork measurements for Case 1. However, the ASHARE standard [31] recommends the minimum ACH value of 20 for the ORs. Therefore, the ACH value of 20 was considered for the OR in the examined Cases of 2 to 6. For the LAF with the air curtain (Case 7), the air velocity of the main diffuser and air curtain, as well as ACH value were considered based on the literature recommendations [11].

The outlet diffusers' layouts were illustrated in Fig. 3 ((a), (b), and (c) represent Cases 2 to 4 as the TAF systems). In Cases 2 to 4, dimensions and room geometry, the surface of inlet diffusers and outlet vents, dimensions, equipment locations, and thermal manikins were considered the same, and only the layout of outlet vents was different. For these cases, four outlet vents were considered for the OR. In Case 2, the outlet vents were planned to be positioned near the floor, and in Case 3, outlet vents were placed opposite each other two by two, as two of them were installed near the ceiling, and others were positioned near the floor. In addition, the outlet vents were located near the ceiling in Case 4.

The effect of inlet diffusers layout was evaluated as the Cases 5 to 7. The inlet diffusers' layouts were also illustrated in Fig. 3 ((d), (e), and (f) represent Cases 5, 6, and 7 as the LAF systems). Cases 5 and 6 present the layouts of 2×2 and 4×1 arrays for the inlet diffusers, respectively, and Case 7 represents the LAF with the air curtain configuration. In Case 7, a surface of diffuser provides the main flow of the OR, and a narrow surface is modeled to create an air curtain around the main diffuser. Case 7 is configured for possible prevention of the environmental contaminants penetration to the critical zone, i.e. the surgical zone (SZ). This layout creates a protective layer around the SZ to prevent contaminants entrance into the SZ. In Case 7, 60% to 75% of the inlet air is provided through the air curtain and the rest through the main diffusers. In Case 7 configuration, the LAF diffuser or main diffuser is usually placed far enough (about 0.3048 m) from the air curtain in order to prevent the LAF penetration into the air curtain and turbulence creation [11]. Besides, based on the ASHRAE standards [32], the main diffuser on the ceiling is recommended to be above the surgical bed with 0.3048 m distance from the sides.

### 2.2 Governing equations

In order to investigate the airflow distribution in the OR space, continuity, momentum, and energy conservation equations are required to be considered.

The continuity equation is [33]:

$$\nabla \cdot \rho \vec{v} = -\frac{\partial \rho}{\partial t} \tag{1}$$

and the momentum equation is [33]:

$$\frac{\partial}{\partial t}(\rho \vec{v}) + \nabla \cdot (\rho \vec{v} \vec{v}) = -\nabla P + \nabla \cdot (\bar{\bar{\tau}}) + \rho \vec{g} \tag{2}$$

and the energy equation is [33]:

$$\frac{\partial}{\partial t}(\rho E) + \nabla \cdot (\vec{v}(\rho E + P)) = \nabla \cdot (\rho K_{eff} \nabla T - h + (\bar{\bar{\tau}}_{eff} \cdot \vec{v})) \tag{3}$$

$E$ is defined as Eq. (4).

$$E = h - \frac{p}{\rho} + \frac{V^2}{2} \tag{4}$$

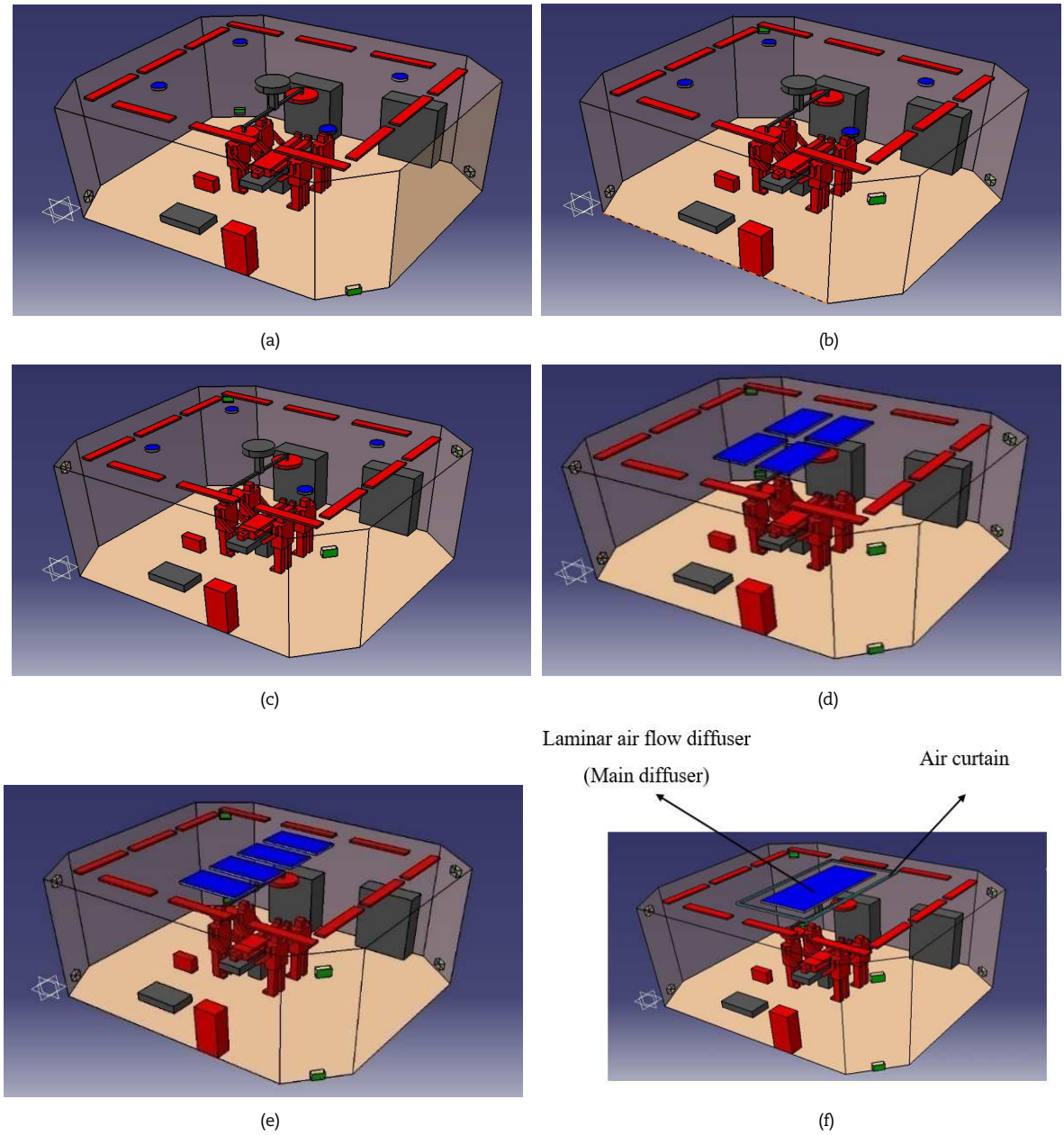


**Fig. 3.** The inlet diffusers' layouts: (a) Case 2; (b) Case 3; (c) Case 4; (d) Case 5; (e) Case 6; (f) Case 7.

Boussinesq approximation is as follows [10]:

$$\rho_{\beta} = \rho_{o}(1 - \beta \cdot \Delta T) \tag{5}$$

In the Boussinesq method, the fluid density is assumed to be a function of temperature. A constant density is assumed in all the equations except for the buoyancy term in the momentum equation. The Boussinesq approximation is defined as the Eq. (5) and the coefficient of thermal expansion (β) is defined as Eq. (6), which is inversely proportional to the temperature of the ideal gas.

$$\beta = -\frac{1}{\rho}\frac{\partial \rho}{\partial T} = \frac{1}{T} \tag{6}$$

The turbulent kinetic energy equation and turbulent kinetic energy dissipation rate are defined as bellow:
The turbulent kinetic energy equation is [10]:

$$\frac{\partial}{\partial x_i}(\rho k u_i) = \frac{\partial}{\partial x_i}\left[(\mu + \frac{\mu_t}{\sigma_k})\frac{\partial k}{\partial x_i}\right] + G_k + G_b - \rho\varepsilon - Y_M + S_k \tag{7}$$

and the turbulent kinetic energy dissipation rate is [10]:

$$\frac{\partial}{\partial x_i}(\rho \varepsilon u_i) = \frac{\partial}{\partial x_i}\left[(\mu + \frac{\mu_t}{\sigma_\varepsilon})\frac{\partial \varepsilon}{\partial x_i}\right] + C_{1\varepsilon}\frac{\varepsilon}{k}(G_k + C_{3\varepsilon}G_b) - \rho C_{2\varepsilon}\frac{\varepsilon^2}{k} + S_\varepsilon \tag{8}$$

**Table 4.** Coefficients of standard k-ε model [10, 22].

| Coefficient | $C_\mu$ | $C_{1\varepsilon}$ | $C_{2\varepsilon}$ | $\sigma_k$ | $\sigma_\varepsilon$ |
|---|---|---|---|---|---|
| Value | 0.09 | 1.44 | 1.92 | 1 | 1.3 |

**Table 5.** Settings for the CFD simulation of the OR.

| | |
|---|---|
| Solver | Pressure based coupled solver and steady state |
| Model | standard $k$-$\varepsilon$ model, standard wall function |
| Boundary condition | As shown in Table 9 & 11 |
| Heat sources | Tabulated in Table 10 |
| Solution method | Scheme: SIMPLE<br>Gradient: least-square cell based<br>Pressure: standard<br>Momentum: second order upwind<br>Turbulent kinetic energy: second order upwind<br>Turbulent dissipation rate: second order upwind<br>Energy: second order upwind |
| Convergence criterion (absolute) | Continuity, x-, y-, z-velocity, k, epsilon: $1\times10^{-3}$, Energy: $1\times10^{-6}$ |

**Table 6.** The resolution, range and accuracy of the anemometer.

| Quantity | Resolution | Range | Accuracy |
|---|---|---|---|
| Velocity | 0.1 m/s | 0.4 to 25 m/s | ± (2% + 2d) |
| Relative humidity | 0.1% | 10% to 95% | ± 3% |
| Temperature | 0.1°C | -50°C to 1300°C | ± (0.4 % + 0.8°C) |

**Table 7.** Fieldwork measurements (supply air conditions).

| Inlet diffuser No. | Temperature (°C) | RH (%) | Velocity (m/s) | Supply airflow rate ($m^3$/h) |
|---|---|---|---|---|
| 1 | 19.9 | 72.5 | 3.4 | 204.81 |
| 2 | 21.8 | 72.6 | 2.2 | 132.53 |
| 3 | 22.3 | 71.4 | 1.2 | 72.29 |
| 4 | 21.1 | 73 | 3.6 | 216.86 |

The coefficients of the standard k-ε model are tabulated in Table 4. The species transport equation is [34]:

$$\frac{\partial(\rho\overline{Y_i u_j})}{\partial x_j} = \frac{\partial}{\partial x_j}((D + D_t)\frac{\partial \overline{Y_i}}{\partial x_j}) + S_i \tag{9}$$

### 2.3 CFD method

In order to simulate the OR space, a CFD code was employed to compute the governing equations. The pressure-based solver was used, and the conservation equations for the steady-state situation were solved using the finite element method. Moreover, the governing equations of momentum, energy conservation, as well as the turbulence were discretized using the second-order method [3, 35].

In the present study, the standard $k$-$\varepsilon$ model was considered for the simulations. In addition, the Boussinesq approximation was used for the natural displacement, and the SIMPLE algorithm was employed for the coupling of pressure and velocity. Moreover, the convergence criteria for continuity, velocity, $k$, and $\varepsilon$ was considered as $1\times10^{-3}$, as well as $1\times10^{-6}$ for the energy [3]. For other species, convergence criteria was considered as $1\times10^{-3}$. The settings for the CFD simulation are presented in Table 5.

### 2.4 Fieldwork measurements

In order to study the indoor air conditions provided by the existing system (Case 1), space air parameters were measured and recorded. The measured data were the supply air temperature, RH, velocity, and airflow rate. The fieldwork measurements were carried out to determine inlet parameters by directly measuring the output of the diffusers. The measurements were conducted on the four vertical axes around the surgical bed, namely Point A, B, C, and D, as illustrated in Fig. 1. The measurements were conducted at the heights of 0.1m, 0.5m, 1m, 1.15m, 1.2m, 1.5m, 1.7m, 2m, 2.5m, and 3m from the floor. In order to eliminate any possible errors, the measurements were conducted in three steps and the mean values were considered. A hot-wire anemometer (model AM-4205A) was used for this purpose. The instrument has been calibrated by equipment already calibrated to international standards. The resolution, range, and accuracy of the anemometer are presented in Table 6.

The required data for the CFD boundary conditions settings, the velocity at the inlet boundaries, and the temperature on the wall boundaries were physically measured. For validation of CFD simulation results, the temperature was measured in four vertical axes, namely A, B, C, and D (Fig. 1). For this purpose, the temperatures of 40 points in the OR space were measured to be compared with the simulation values. Moreover, to model the RH parameter, the initial value of the RH was required. Therefore, RH values were measured, and the mean value was considered for the simulations. The fieldwork measurement was conducted several times to avoid any possible errors. The fieldwork measurements are tabulated in Table 7.

**Table 8.** The axes coordinates for the mesh independence examination.

| Axis | Coordinate | |
|---|---|---|
| | X | y |
| E | 2.34 | 2.85 |
| F | 3.09 | 1.2 |
| G | 3.84 | 2.85 |

**Table 9.** Boundary condition for the space walls.

| Wall | N | S | E | W | C | F | N.E | N.W | S.E | S.W |
|---|---|---|---|---|---|---|---|---|---|---|
| Temperature (°C) | 22.6 | 22.1 | 22.3 | 22.5 | 22.3 | 22.2 | 22.2 | 22.3 | 22.5 | 22.5 |

[N]Northern, [S] Southern, [E] Eastern, [W] Western, [C] Ceiling, [F] Floor, [N.E]Northeast, [N.W]Northwest, [S.E]Southeast, [S.W]Southwest.

### 2.5 Mesh independence

A suitable mesh number is a deciding factor for the simulation process, and the results of a CFD simulation strongly depend on the quality of the considered computational mesh [11]. Therefore, in order to select a proper mesh number for the numerical simulations, it is necessary to investigate the mesh independence first (Note: the tetrahedral mesh type was employed for this purpose.). The OR model under the four different mesh number, namely, 672,979; 885,097; 1,007,432; 1,120,195 were investigated and analyzed around the surgical bed. Three vertical axes – E, F, and G – were examined for this purpose (see Fig. 1). The axes coordinates are presented in Table 8.

Fig. 4 illustrates the generated mesh for the room model. The considered mesh is unstructured mesh type, and it is due to the complexity of the geometry. The mesh generation is such that in high-gradient areas such as inlet diffusers, outlet vents, walls, proximity of equipment and thermal resources and especially in SZ, the mesh numbers increase in order to solve the effects of each with high accuracy.

Fig. 5 illustrates the pressure variation for the considered mesh numbers. As it was illustrated in Fig. 5, the parameter variation for the mesh number of 1,007,432 and 1,120,195 cells are not significant, and the graphs are matched; therefore, the mesh number of 1,007,432 cells was considered for the model and the simulations.

### 2.6 Boundary conditions

Boundary conditions are major factors for the reliability of CFD simulation results. A realistic and accurate implementation of the boundary conditions is an essential part of any CFD simulation. The proper numerical and physical behavior of the boundaries will affect the accuracy of computations as well as the convergence time. In this study, the boundary conditions were determined based on the fieldwork measurements. The supply air condition was modeled as a mixture of dry and vapor air without any chemical reactions [22]. The supply air enters into the OR space via the ceiling's diffusers in the downward vertical direction. It was assumed that $CO_2$ as the only breathing contaminant by the patient and surgical team releases in a mass fraction of $2\times10^{-4}$ (200 ppm) [22] and flow rate of eight liters per minute [36].

Since the operating room is located between two adjacent rooms and the temperature difference between the spaces was negligible, the constant temperature boundary condition was assumed for the walls. The surface temperatures of the walls were determined by direct measurements. Table 9 presents the boundary conditions considered for the walls based on the fieldwork measurements. Human models perform as the heat sources, and their thermal effects must be considered. Medical equipment in the OR, such as the anesthesia machine, patient care monitor, ceiling lamps, and surgical lights, also need to be considered as the heat sources. The generated heat values were obtained from the available data and fieldwork measurements. The heat source items in the modeled OR are tabulated in Table 10. Table 11 represents the inlet boundary conditions for the designed cases. It must be noted that the boundary conditions for Case 1 were based on the fieldwork measurements.

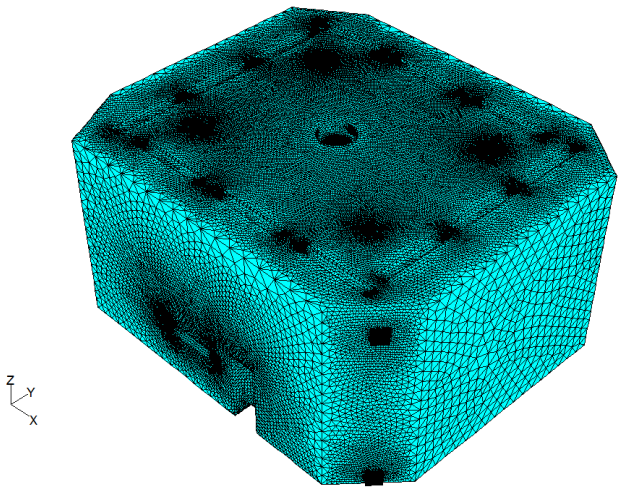


**Fig. 4.** Generated mesh for the room model.

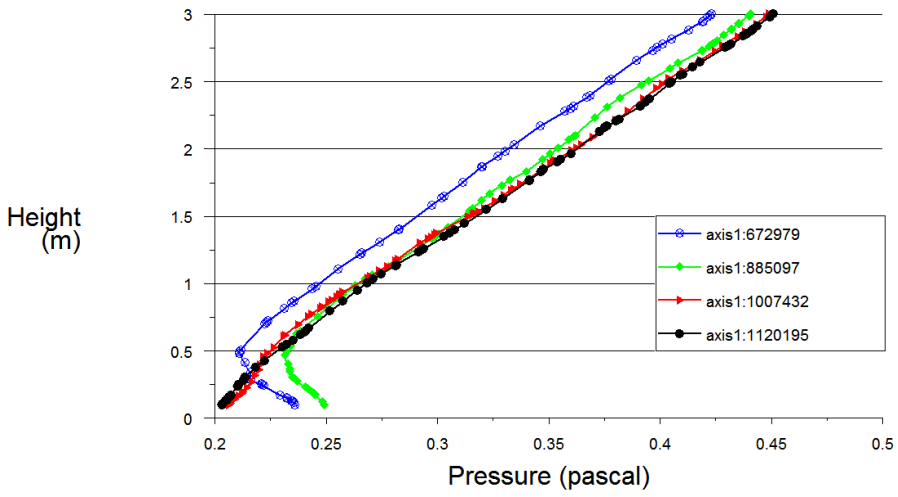


(a)

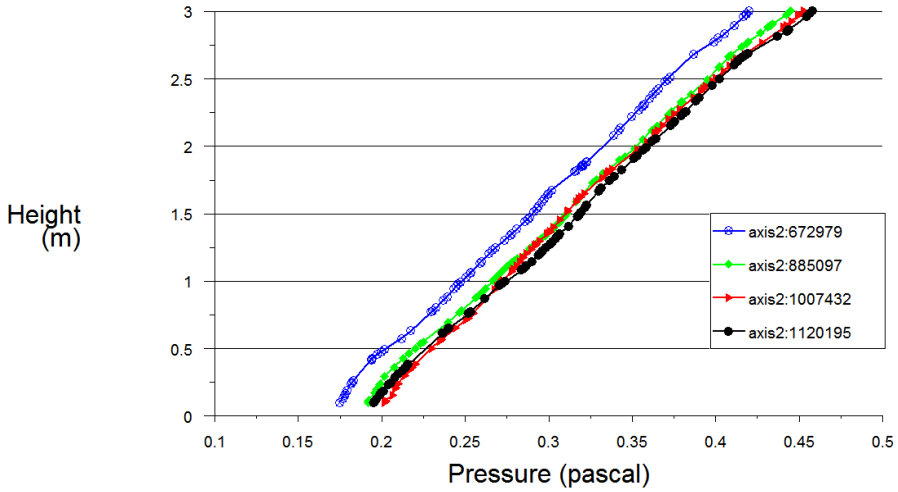


(b)

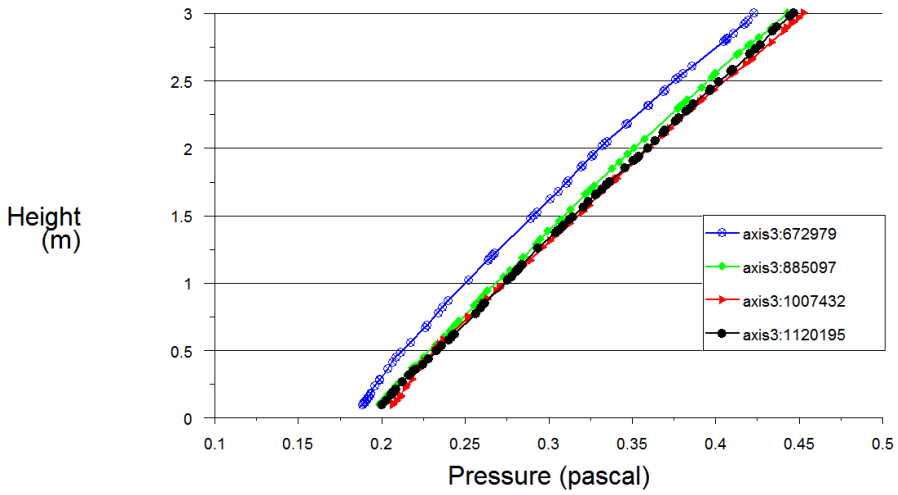


(c)

**Fig. 5.** Pressure variation at different mesh numbers: (a) axis E; (b) axis F; (c) axis G.

**Table 10.** Heat sources in the OR space.

| Item | Quantity | Heat source (W) |
|---|---|---|
| Surgical team | 4 | 100 |
| Patient | 1 | 75 |
| Anesthesia machine | 1 | 200 |
| Patient care monitor | 1 | 100 |
| Each pair of lamps | 12 | 16 |
| Surgical lights | 2 | 42 |

**Table 11.** Boundary condition for the inlet diffusers.

| Case number | Boundary | Velocity (m/s) | Temperature (°C) | RH (%) |
|---|---|---|---|---|
| Case 1 | Inlet 1 | 3.4 | 19.9 | 72.5 |
| | Inlet 2 | 2.2 | 21.8 | 72.6 |
| | Inlet 3 | 1.2 | 22.3 | 71.4 |
| | Inlet 4 | 3.6 | 21.1 | 73 |
| Case 2 & Case 3 & Case 4 | Inlets | 2.6 | 18.3 | 72.4 |
| Case 5 & Case 6 | Inlets | 0.2 | 18.3 | 72.4 |
| Case 7 | Main diffuser | 0.127 | 18.3 | 72.4 |
| | Air curtain | 1.14 | | |

**Table 12.** The range of air parameters in the OR [31, 32].

| Temperature (°C) | RH (%) | Velocity (m/s) | Pressure | Minimum ACH |
|---|---|---|---|---|
| 20-24 | 20-60 | 0.13-0.18 | positive | 20 |

**Table 13.** Coordinates of validation axes.

| Axis | Coordinate | |
|---|---|---|
| | X | Y |
| A | 2.24 | 1.866 |
| B | 3.94 | 1.866 |
| C | 3.94 | 3.846 |
| D | 2.24 | 3.846 |

### 2.7 ASHRAE standard

The ASHRAE standard provides specific guidelines and requirements for the design and operation of ORs. This standard specifies the range of air parameters such as temperature, humidity and velocity, pressure, and minimum ACH value for the ORs (Table 12).

## 3. Results and Discussions

In this section, the simulation results are presented and discussed. The air parameters such as temperature distribution, RH distribution, velocity distribution, and $CO_2$ concentration will be discussed for the examined cases in the subsections.

### 3.1 Validation

In order to validate the simulation results, the simulation values were compared with the fieldwork measurement. Validation was conducted for the existing model (i.e., Case 1), which is a TAF-based case. In this study, the validation of the model was conducted based on the temperature and RH values on the four axes of A, B, C, and D. The coordinates of the axes are tabulated in Table 13.

The comparison of the fieldwork measurements and the simulation values for temperature are presented in Fig. 6. As it was illustrated in Fig. 6, there was an acceptable accuracy for the simulation values, with a maximum deviation of 3.08%. In order to further improve the credibility of the simulations, the validation for the RH value was also conducted (Fig. 6). The comparison between the fieldwork measurements and simulation values for the RH parameter showed an acceptable deviation between the fieldwork measurement and simulation values, with a maximum deviation of 7.82%.

### 3.2 Temperature distribution

Fig. 7 shows the temperature distribution for plane Z at the 1.14 meter above the floor, as the approximate distance for a patient. In all the examined cases, temperature distribution around the heat sources, such as the anesthesia machine and the patient care monitor was found to be high. Since these instruments produce a high amount of heat, a thermal mass was created around these devices. The study showed that in Case 1 (existing system), the established maximum temperature is higher than the maximum temperature observed by the other examined cases due to the low ACH value and high static flow situation. In addition, it was found that in Case 2, where all the outlets are installed at the bottom, most of the inlet flow moves directly to the outlets and leaves the space without making any cooling leading to an increase in the temperature around the heat sources.

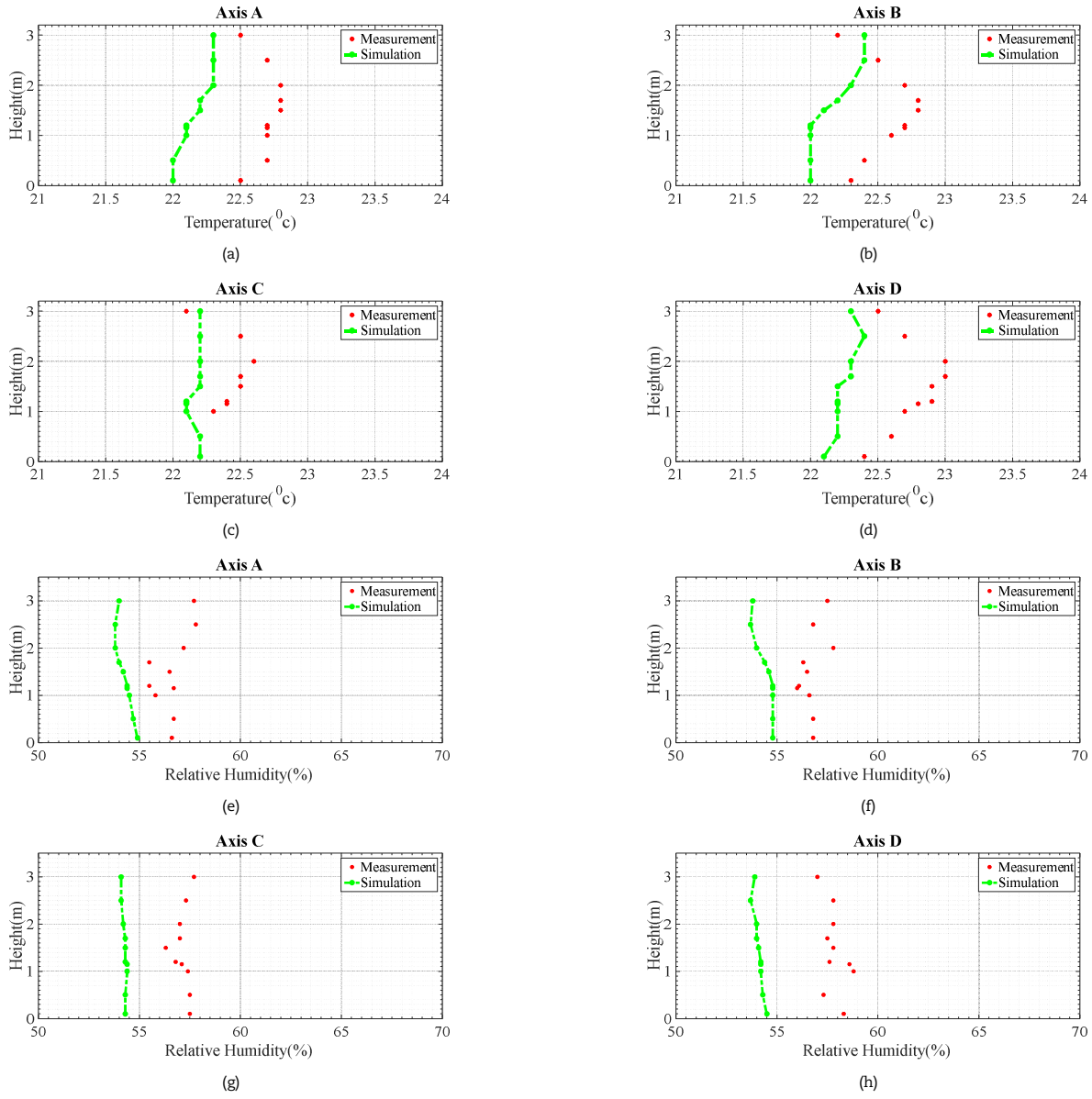


**Fig. 6.** Comparison of the fieldwork measurements and simulation values for temperature: (a) axis A; (b) axis B; (c) axis C; (d) axis D and relative humidity: (e) axis A; (f) axis B; (g) axis C; (h) axis D.

The simulation revealed that for the Cases 2 to 4, as the layout of the outlet patterns, the temperature distribution in the space outside the SZ obeys almost the same pattern for all the cases, and variations were not observed in the zone for different cases. Based on the simulation, the temperature is about 20°C, which is within the range recommended by the ASHRAE standards [31].

The study showed that the temperature distribution pattern is different in the SZ for the examined cases, and this is mainly due to the heat generation by the thermal mannequins. In Cases 1 to 4, as the TAF-based cases, the patient experiences a high-temperature value of about 30°C, which is outside the range recommended by the ASHRAE standards [31]. However, Cases 5 to 7, as the LAF-based and LAF with the air curtain cases, could provide an appropriate temperature distribution for the SZ and patient, and the surgical team experiences temperature values within the range recommended by the standards.

By considering all the above, it is concluded that the performances of LAF-based and LAF with the air curtain cases are more desired than TAF-based cases in terms of provided temperature for the SZ.

Fig. 8 shows the temperature distribution in the space for different X-planes. These planes were considered as the representative to illustrate the temperature distribution pattern in the whole space. As it was shown in Fig. 8, the temperature around the heat sources increases due to the heat generation. By comparing TAF-based cases (Cases 1 to 4), it was observed that Case 3 establishes a lower maximum temperature than other TAF-based cases. In other words, Case 3 is the desired configuration to keep the maximum temperature down enough in the apace. The comparison of TAF based cases performance (i.e., Cases 1 to 4) with LAF-based and LAF with the air curtain cases (i.e., Cases 5 to 7) proved that LAF-based and LAF with the air curtain cases are more desired than TAF-based cases in terms of keeping down space maximum temperature. According to the simulation results, the LAF-based and LAF with the air curtain cases have the capability to establish temperature value about 8°C lower than TAF based cases provided value.

The study showed that the temperature variation in planes of X = 1.54 m and X = 4.873 m (these two planes are the planes excluding the SZ) was negligible in the vertical direction for Cases 2 to 4; while the variation along the Y-direction was observed. However, in Cases 5 to 7, the temperature variation along the Y-axis is negligible, whereas a variation along the vertical being observed.

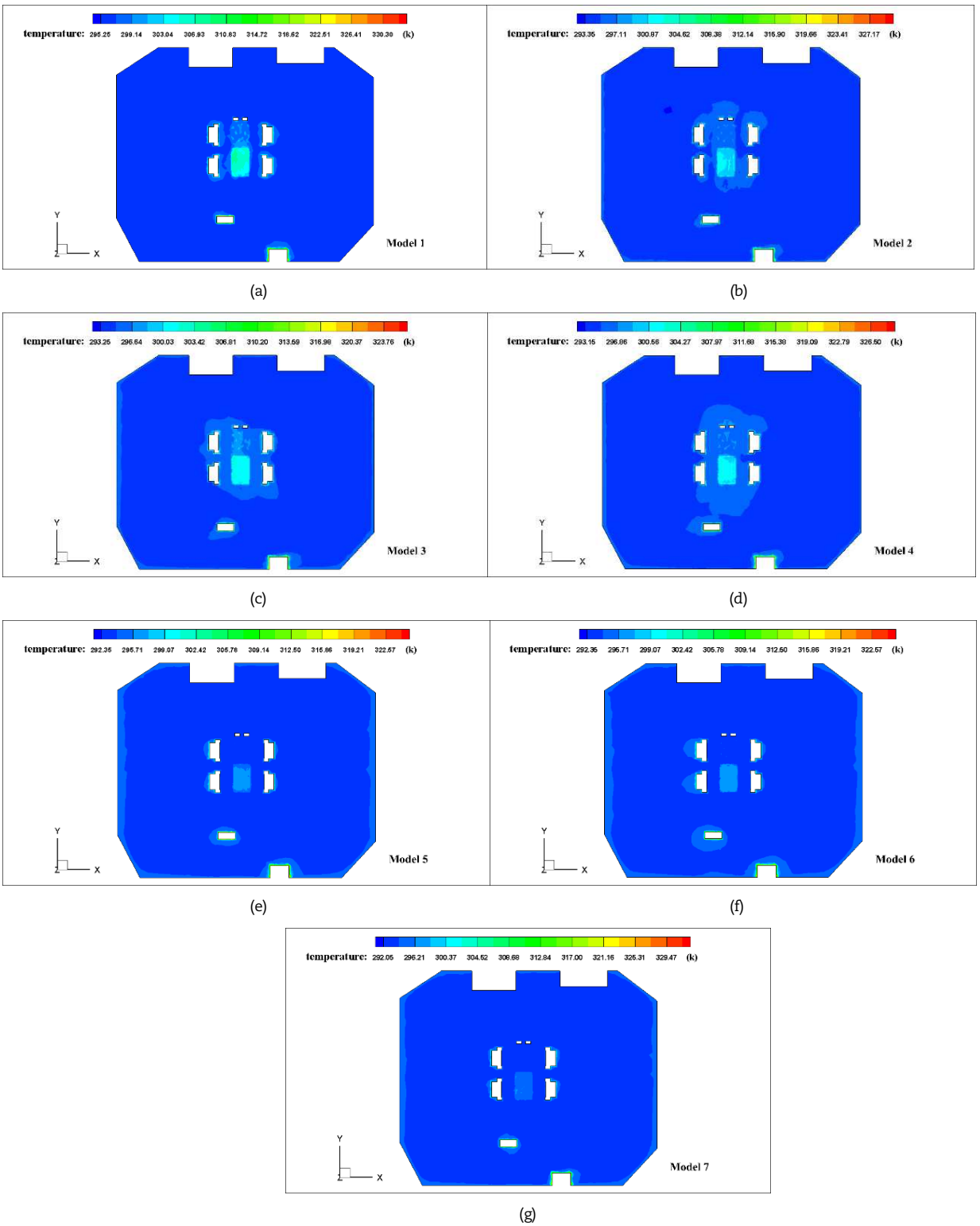


**Fig. 7.** Temperature distribution in plane Z = 1.14 m: (a) Case 1; (b) Case 2; (c) Case 3; (d) Case 4; (e) Case 5; (f) Case 6; (g) Case 7.

The assessment of the temperature distribution in the central plane, as the plane passes through the SZ, indicates that in the TAF-based cases (Cases 1 to 4), the temperature around the patient and the surgical team increases and makes the patient be exposed to high-temperature values. However, LAF-based and LAF with the air curtain cases (Cases 5 to 7) provide a desired temperature distribution for the SZ, and the patient and surgical team experience an acceptable temperature of about 20°C.

### 3.3 RH distribution

RH value is one of the major parameters in occupants' thermal comfort. In addition, the higher RH values would lead to the growth and distribution of microorganisms and infections in the space, [37]. The ASHRAE [31] standard recommends an RH range of 20% to 60% for the ORs. Therefore, RH distributions on the different planes inside the OR, including the patient body and surgical team, were evaluated in the present research (Figs. 9 and 10). The study showed that in Case 1, as the existing system, the RH is distributed uniformly in the OR space. In Case 1, the temperature rises in the room due to the low ACH value and airflow durability in the space. As it is illustrated in Fig. 9, the RH distribution in the space outside the SZ is in the range of 48% to 54%. It was shown that for this case, the patient and the surgical team experience RH values about 40% to 48%.

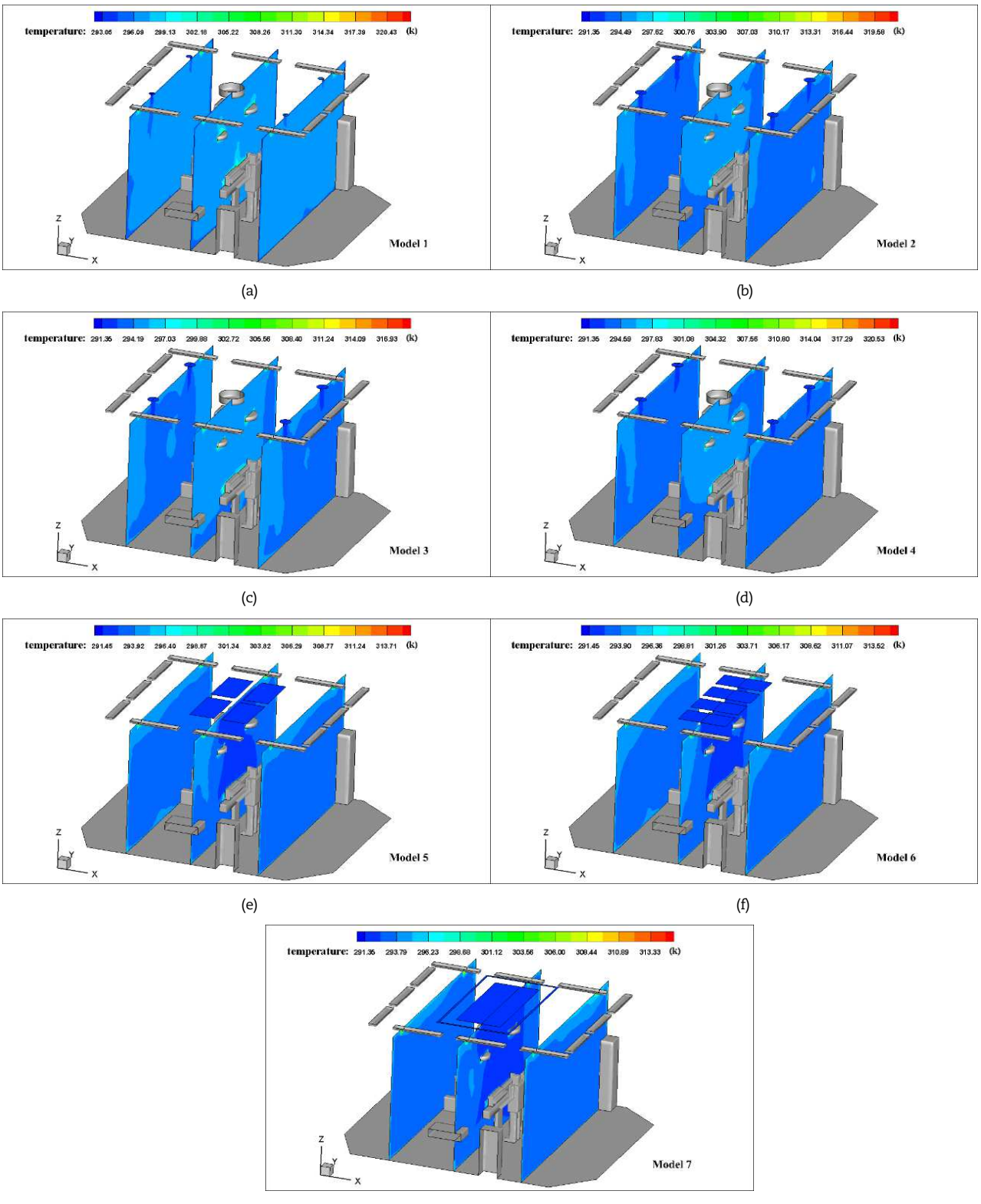


**Fig. 8.** Temperature distribution in planes X = 1.54 m, X = 3.17 m and X = 4.873 m: (a) Case 1; (b) Case 2; (c) Case 3; (d) Case 4; (e) Case 5; (f) Case 6; (g) Case 7.

Based on the simulation results, in Cases 2 to 4, an uneven RH distribution was observed, and the patient and the surgical team were exposed to the RH values of about 45% to 55%. It was also found that in LAF-based and LAF with the air curtain cases (Cases 5 to 7), the patient and the surgical team experience RH values in the range of 50% to 65%; hence, the RH distribution in Cases 5 to 7 is high for the SZ. The RH values tend to surpass the 60%, which is not within the range recommended by the standard. The comparison of RH distribution provided by the TAF-based cases (Cases 1 to 4) with that provided by LAF-based and LAF with the air curtain cases (Cases 5 to 7) shows that TAF-based cases could provide RH values within the lower range of the standard recommendations. In addition, it was also found that LAF-based and LAF with the air curtain cases have the capability to establish a more uniform RH distribution than the TAF-based cases for the SZ. However, in these cases (Cases 5 to 7), the RH values tend to surpass 60%, which is not within the range recommended by the standard. Moreover, the distribution pattern indicates that Case 1 could provide the most appropriate RH distribution for the OR space.

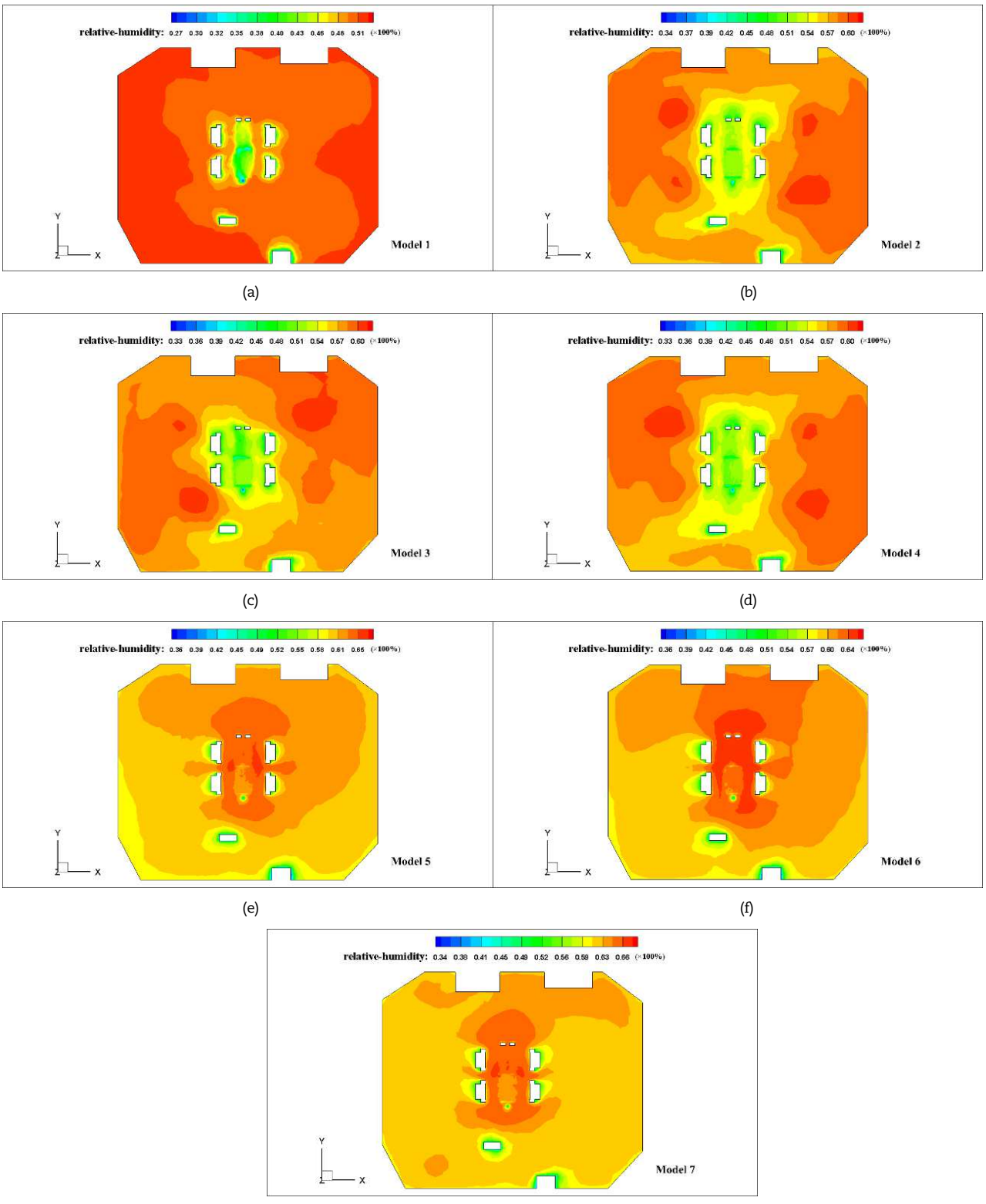


**Fig. 9.** RH distribution in plane Z = 1.14 m: (a) Case 1; (b) Case 2; (c) Case 3; (d) Case 4; (e) Case 5; (f) Case 6; (g) Case 7.

Fig. 10 shows the RH distribution for the various X-planes in the OR space. As shown in Fig. 10, the RH value decreases as the air flows downwards and mixes with the air inside the space. In Cases 1 to 4, the inlet diffusers are located just above the planes, excluding the SZ. As illustrated in Fig. 10, the RH value decreases as getting away from the inlet diffusers. The variation is considerable in the Y-direction. However, in Cases 5 to 7, in the planes excluding the SZ, the RH variation along the Y-dire ction is negligible, while the RH variation along the Z-direction is observed as approaching to the OR ceiling. In Cases 1 t o 4, the RH distribution in the central plane is at lower values than the inlet values. As mentioned before, in Cases 1 to 4, the central plane is far from the inlet diffusers, and the inlet air RH value decreases as it flows through the SZ. There fore, the patient and the surgical team experience low RH values. Based on the simulation results, the RH values provided by Cases 5 to 7 are higher than the values established by Cases 1 to 4, and this is because of the fact that the inlet diffusers are located just above the central plane. In Cases 5 to 7, the airflow is supplied directly to the SZ and consequently makes the patient and the surgical team experience a high level of RH values.

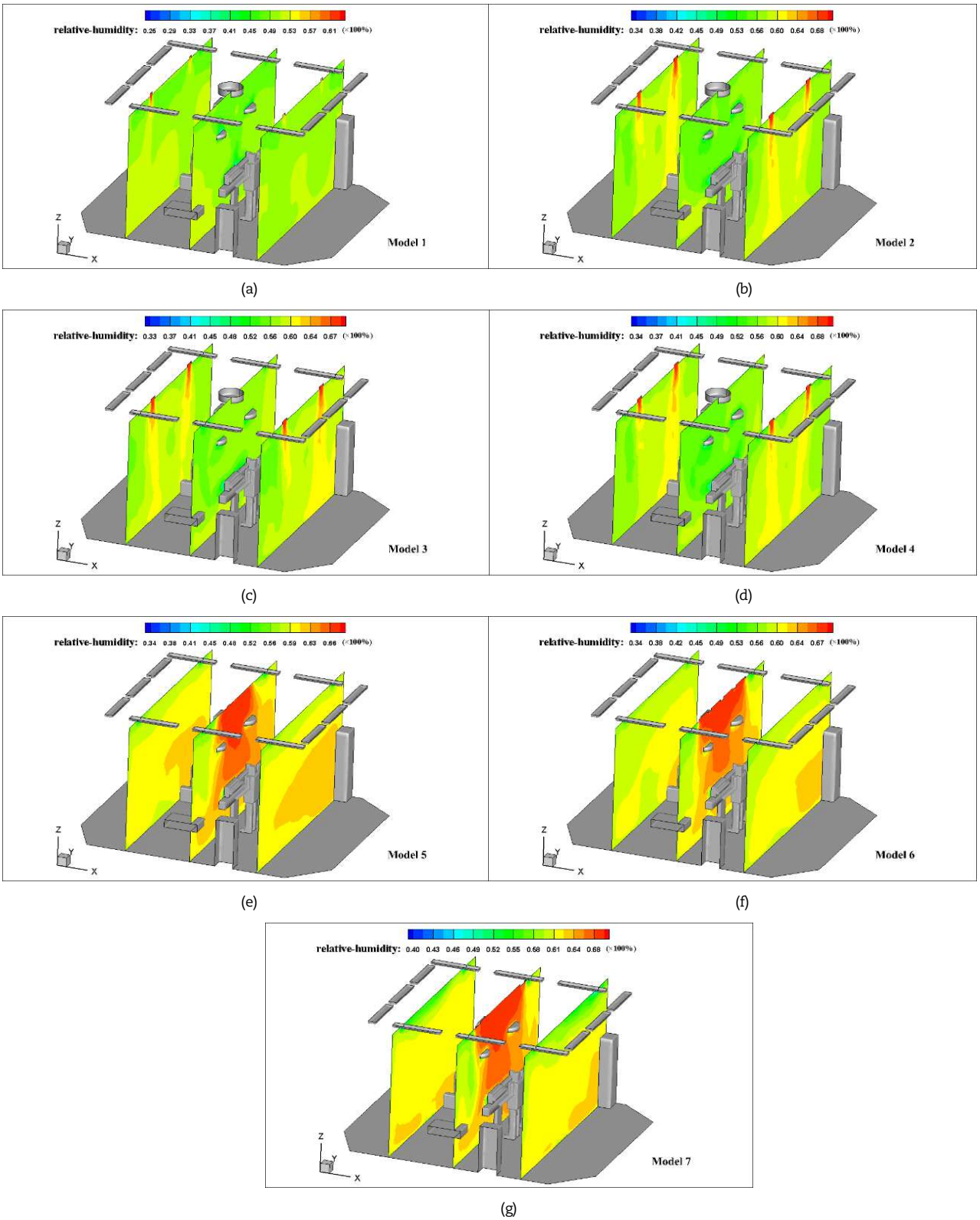


**Fig. 10.** RH distribution in planes X = 1.54 m, X = 3.17 m and X = 4.873 m: (a) Case 1; (b) Case 2; (c) Case 3; (d) Case 4; (e) Case 5; (f) Case 6; (g) Case 7.

### 3.4 Airflow velocity distribution

Fig. 11 shows the airflow velocity distribution about one meter above the floor (the plane Z = 1.14 m). In Fig. 11, the colored regions represent the negative-velocity vector (towards the floor), and the non-colored regions represent the positive velocity vector (towards the ceiling).

In Case 1 as the existing condition, different velocity values were observed just below the inlet air diffusers, which proves the lack of proper velocity distribution in the area. As illustrated in Fig. 11, the velocity value below the diffuser No. 4 is the maximum and for the diffuser No. 3 is the minimum. The upward airflow direction in the SZ was observed in this case. It was also found that the upward flow in the surgical team's occupied region was dominant in Cases 2 to 4. Therefore, it can be concluded that the airflow patterns established by Cases 1 to 4, were upward, except for the inlet diffusers and their surrounding areas. It was also observed that only a small fraction of the flow in the SZ was downward.

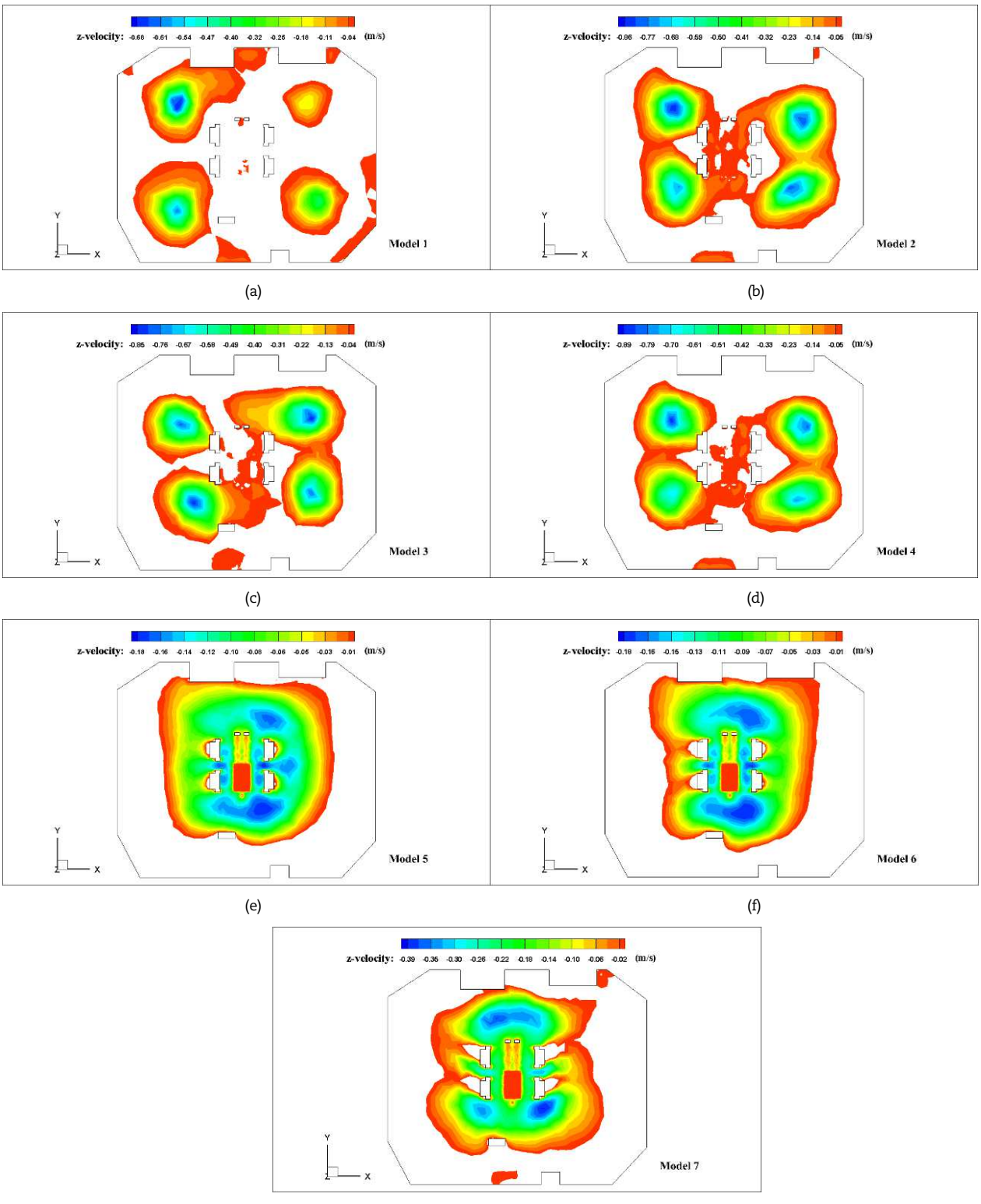


**Fig. 11.** Distribution of the z-component of velocity in the plane Z = 1.14 m: (a) Case 1; (b) Case 2; (c) Case 3; (d) Case 4; (e) Case 5; (f) Case 6; (g) Case 7.

The study revealed a different performance by Cases 5 to 7 for the velocity distribution. The study showed that the flow direction provided by the Cases 5 to 7 was upward for the space outside SZ; however, due to the direct flow supply in the SZ, the airflow in this area is mostly downward, which makes the patient and the surgical team to be under a unidirectional and downward flow condition.

Fig. 12 shows the velocity distribution for the X-planes. As it is presented in Fig. 12, in Cases 1 to 4 (TAF-based cases), where the inlet diffusers are directly above the planes excluding the SZ, the velocity below the diffusers has its maximum value along the vertical direction. High-velocity values established by these cases (Cases 1 to 4) make particles turbulence and disturbance to increase around the inlet diffusers, and as a result, the risk of contamination and infection may increase. In Cases 1 to 4, the established velocity values in the SZ is less than the values in the surrounding area, and therefore, the flow velocity is low for the central plane passing through the SZ. This performance of airflow in the SZ in terms of velocity makes the flow to be static. As a result, particle's movement would be affected, and the high risk of contamination is expected. As already explained, the inlet diffusers are located directly above the SZ in Cases 5 to 7 as the LAF-based and LAF with the air curtain cases. In these

configurations, the inlet air directly approaches the patient and the surgical team, exposing them to a fresh air supply. The proper supply air velocity by these cases for the SZ has resulted in lower flow stagnation than the TAF-based cases (Cases 2-4) in the zone, and the infection risk would be minimized. Case 7, as the LAF-based case with the air curtain, was also illustrated in Fig. 12. In this configuration, the high velocity of linear diffuser establishes an air curtain around the SZ and prevents the penetration of the contaminants into the SZ and protects the patient and the surgical team against the external contaminants.

The surgical lights are directly located below the inlet diffusers in Cases 5 to 7; therefore, they create a physical barrier for the supply air. This physical barrier affects the airflow direction. The airflow rotation and its stagnation under surgical lights prevent the particle's movement and increase the possibility of particle concentration in this area. The velocity patterns provided in the planes excluding the SZ by Cases 5 to 7 are within a suitable range; however, a rotational flow pattern was also observed in these areas, which may increase the contamination risk. In general, it can be concluded that LAF-based and LAF with the air curtain cases have the capacity to establish a more desired velocity distribution than TAF based cases.

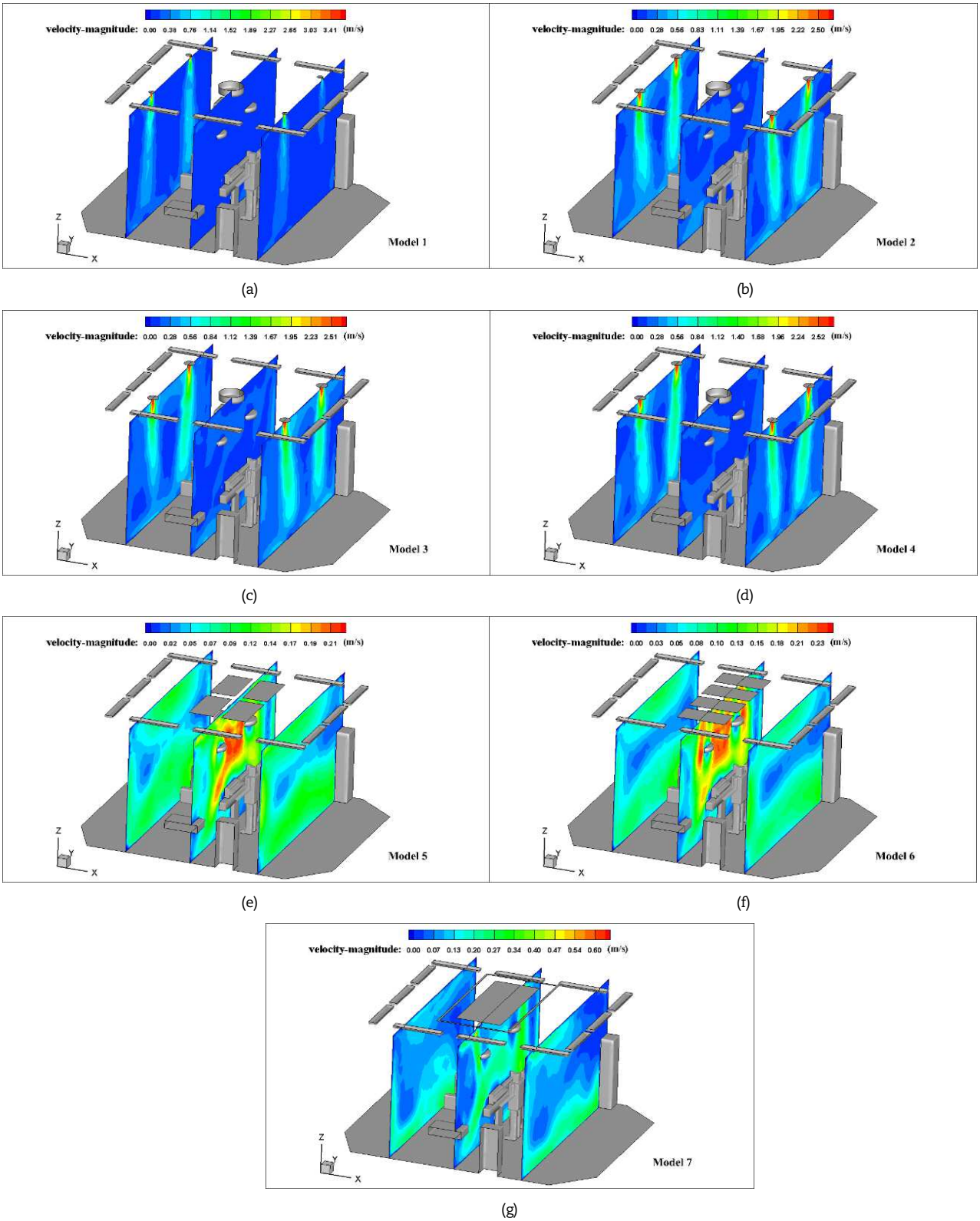


**Fig. 12.** Velocity distribution in planes X = 1.54 m, X = 3.17 m and X = 4.873 m: (a) Case 1; (b) Case 2; (c) Case 3; (d) Case 4; (e) Case 5; (f) Case 6; (g) Case 7.

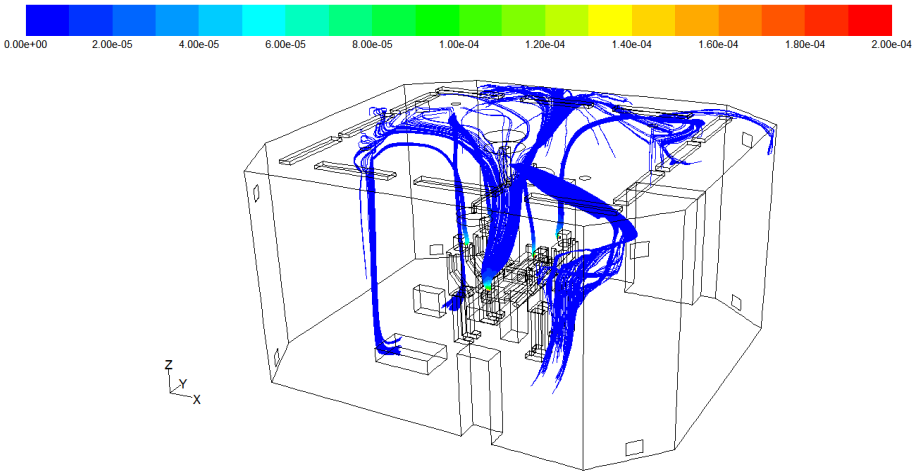


**Fig. 13.** $CO_2$ path lines for Case 1.

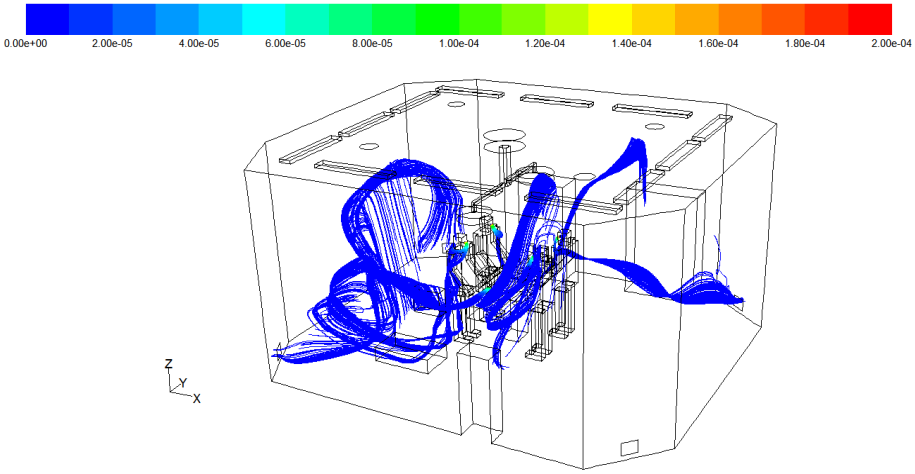


**Fig. 14.** $CO_2$ path lines for Case 2.

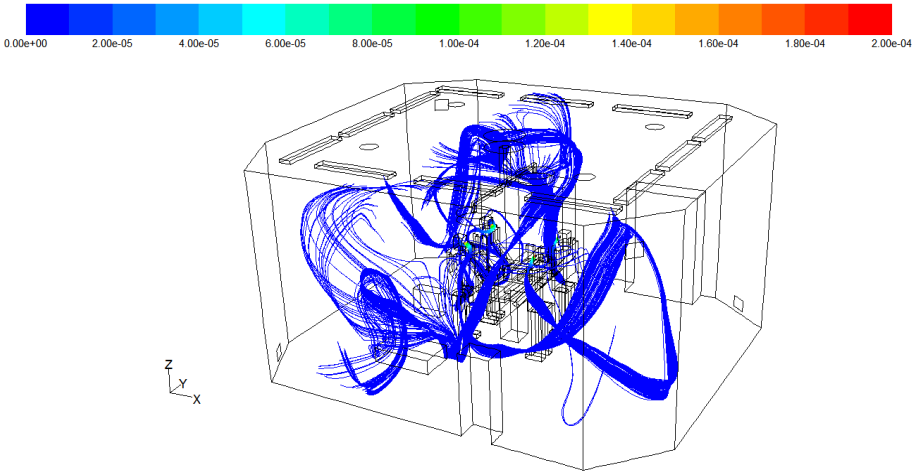


**Fig. 15.** $CO_2$ path lines for Case 3.

### 3.5 Path lines of the occupants' respiratory flow ($CO_2$ path lines)

Figs. 13-19 illustrate the path lines of the occupants' respiratory flow ($CO_2$ path lines) for the examined cases. As illustrated in Fig. 13, in Case 1 (existing condition), the occupants' respiratory flow in the SZ mixes with the fresh air causing the inlet air to be contaminated.

Figs. 14-16 show the occupants' respiratory flow for Cases 2 to 4. As shown in these patterns, the occupants' respiratory flow is transmitted to the outside region of the SZ; consequently, it decreases the concentration of contaminants in the SZ compared to the situation established by Case 1. Moreover, in Case 2 (see Fig. 14), since a significant part of the occupants' respiratory flow moves directly to the outlet diffusers, the concentration of contaminants in the SZ is lower than the situation provided by Cases 3 and 4.

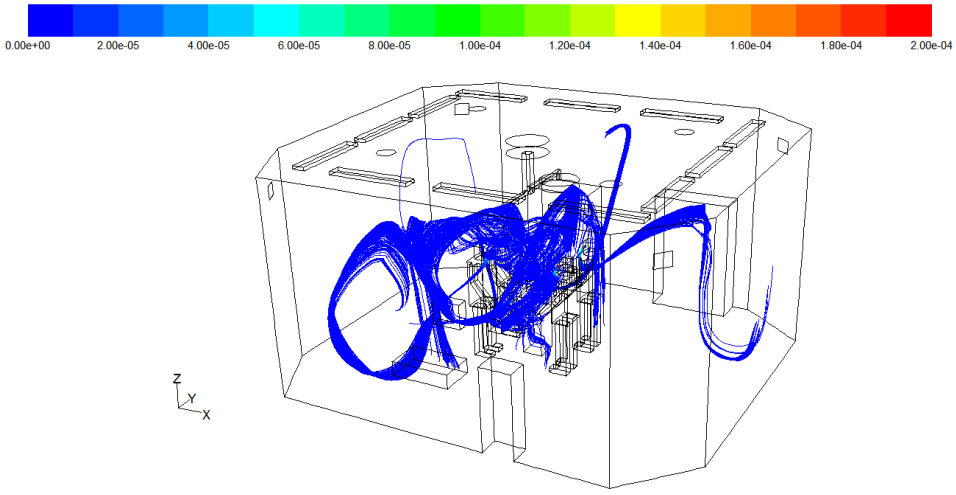


**Fig. 16.** $CO_2$ path lines for Case 4.

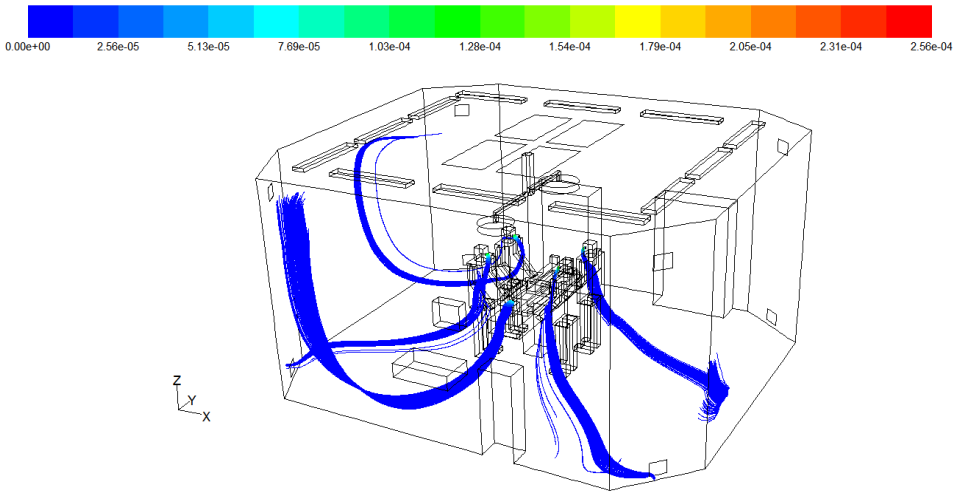


**Fig. 17.** $CO_2$ path lines for Case 5.

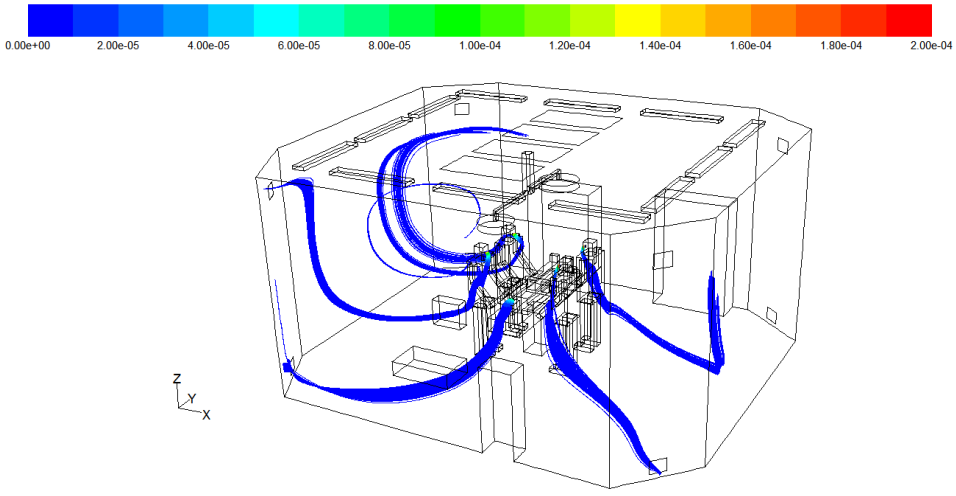


**Fig. 18.** $CO_2$ path lines for Case 6.

The occupants' respiratory flow path lines established in Cases 5 to 7 show more efficient patterns (Figs. 17-19). As it is shown in Figs. 17-19, the occupants' respiratory flow is directly drawn out of the SZ and prevents the respiratory particles accumulation in the zone.

It was also revealed that Case 7, as the LAF-based case with the air curtain, is the most desired configuration in terms of minimizing the concentration of contaminants in the SZ. In Case 7 configuration, the air curtain in the SZ, functions as a physical barrier and prevents the environmental contaminants and reversed occupants' respiratory flows from entering into the SZ (see Fig. 19).

**Table 14.** The mean values of $CO_2$ concentration established by the Cases.

| Case | Concentration (ppm) | | | | | | |
|---|---|---|---|---|---|---|---|
| | Patient | Surgeon | Anesthetist | Nurse 1 | Nurse 2 | Z = 1.14 | Z = 1.7 |
| Case 1 | 22.30 | 16.59 | 17.86 | 17.99 | 18.30 | 3.36 | 5.08 |
| Case 2 | 18.90 | 14.28 | 15.77 | 14.25 | 15.92 | 1.61 | 0.89 |
| Case 3 | 20.06 | 15.28 | 16.56 | 14.17 | 17.75 | 1.82 | 1.26 |
| Case 4 | 18.90 | 14.67 | 15.06 | 14.22 | 17.06 | 1.78 | 1.05 |
| Case 5 | 18.48 | 13.68 | 13.82 | 13.66 | 14.24 | 1.38 | 0.70 |
| Case 6 | 18.92 | 14.01 | 15.35 | 13.93 | 15.36 | 1.37 | 0.68 |
| Case 7 | 17.64 | 13.13 | 13.51 | 12.70 | 13.32 | 1.08 | 0.38 |

### 3.5.1 The $CO_2$ concentration

Table 14 presents the mean $CO_2$ concentration values for the patient and personnel. The two vertical distances from the floor, for the patient and surgical team, as the planes Z = 1.14 m and Z = 1.7 m, were considered for this purpose. As tabulated in Table 14, Case 1 (existing condition) establishes the highest values of $CO_2$ concentration, and this is due to the lack of ACH rate and non-effective control on the flow pattern. In Case 1, the mean $CO_2$ concentration value on the patient's body and in the patient's breathing region is 22.30 ppm and 3.36 ppm, respectively. As tabulated in Table 14, by configuring the output layouts as the Cases 2 to 4, the $CO_2$ concentration value has been significantly reduced. It was also found that for the TAF-based cases (Cases 1 to 4), Case 2 could establish the most desired values for the $CO_2$ concentration in the patient's breathing region. In this case, the mean $CO_2$ concentration on the patient's body and in the patient's breathing region is 18.90 ppm and 1.61 ppm, respectively.

The performance of the LAF-based and LAF with the air curtain cases (Cases 5 to 7) in terms of $CO_2$ concentration was also tabulated in Table 14. It was found that the LAF-based and LAF with the air curtain cases (Cases 5 to 7) have the potential to provide a more appropriate distribution of $CO_2$ concentrations than the TAF-based cases (Cases 1 to 4). Moreover, it was proved that the most appropriate case is the LAF with the air curtain as Case 7. In Case 7, the established mean $CO_2$ concentration on the patient's body and the patient's breathing region is 17.64 ppm and 1.08 ppm, respectively. Case 7 configuration could keep the patient and the surgical team from the risk of infection by creating a more sterile space for the SZ.

In the examined cases, the $CO_2$ concentration is less than the legal limitations (1500 ppm). However, for the success of surgical procedures, the concentration of pollutants in the operating room must be at its lowest level. Therefore, different cases were examined to suggest a case that creates the lowest concentration of pollutants in the OR. The examination of $CO_2$ concentration shows that Case 7 configuration establishes the lowest $CO_2$ concentration levels in the OR. It was also found that Case 7 has the capability to reduce the $CO_2$ concentration value about 20.90%, 20.86%, 24.36%, 29.41%, 27.21%, 67.86%, 92.52% for the patient, surgeon, anesthetist, nurse 1 , nurse 2, Z = 1.14 m and Z = 1.7 m, respectively compared to Case 1.

## 4. Conclusions

In the present research, the performance of the existing HVAC system in an OR in terms of indoor air conditions and air distribution patterns were studied. Different configurations for the inlet and outlet diffusers as the six different cases were examined to explore the possible improvements in the HVAC system's performance. CFD method was employed for this purpose, and three methods of turbulent airflow (TAF), laminar airflow (LAF), and LAF with the air curtain methods were considered.

The findings are presented below:

i. The fieldwork study and simulations revealed that the temperature distribution of the existing system of the OR could not establish a desired temperature distribution for the OR space. It was shown that due to the low ACH value and static flow in the existing case, high values of temperature were provided for the OR space.
ii. The temperature distribution established for the SZ by the TAF-based cases is non-uniform, and the patient and the surgical team are exposed to high-temperature values, while the LAF-based and LAF with the air curtain cases could provide more uniform temperature distributions than the patterns established by the other examined cases for the SZ, and the patient and the surgical team are exposed to an appropriate temperature of 20°C.
iii. The RH distribution in the existing case and the LAF with the air curtain cases has more uniformity than in the other examined cases. However, the existing case is the desired case to create appropriate RH values in the space and for the SZ in particular.
iv. The air velocity distribution by TAF-based cases was inappropriate, and a stagnant space was created in the SZ by the TAF-based cases. However, the LAF-based and LAF with the air curtain cases have the capability to provide an appropriate air velocity distribution for the SZ.
v. The Maximum $CO_2$ concentration for the OR space and especially for the SZ, was observed in the existing case, and it proves the inefficient operation of the existing ventilation system. It was also found that the LAF with the air curtain case has the capability to establish the most appropriate level of contaminant's concentration.

By considering all the above, it can be concluded that the LAF and LAF with the air curtain cases are the most suitable cases for establishing comfortable conditions for the OR. Among the examined cases, the LAF with the air curtain as the proposed case is the best configuration in terms of the contamination risk and creates a more sterile environment for the OR.

## Author Contributions

The present research was conducted by V. Gholami Motlagh as a postgraduate student under the supervision of M. Ahmadzadehtalatapeh as the supervisor.

## Acknowledgments

The authors would like to acknowledge Chabahar Maritime University (CMU), Iran and Chabahar Iranian Surgery Clinic, Chabahar for their cooperation during the research.

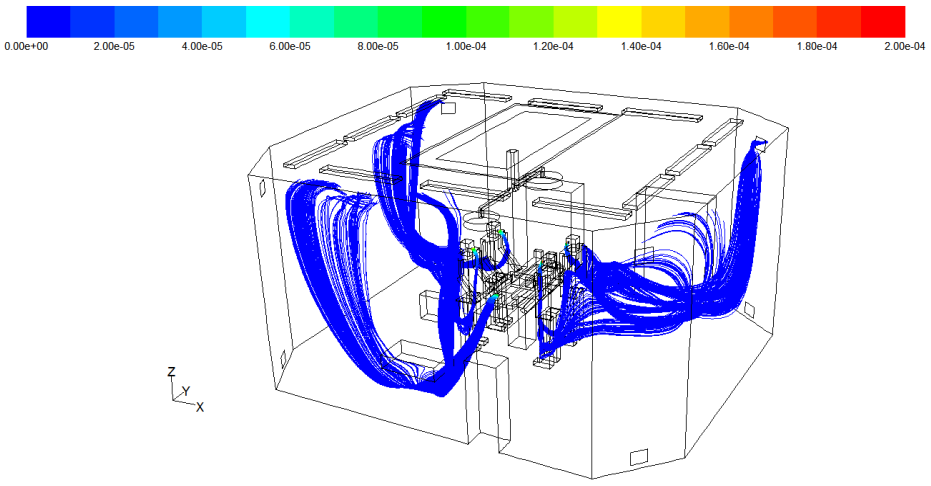


**Fig. 19.** $CO_2$ path lines for Case 7.

## Conflict of Interest

The authors declared no potential conflicts of interest with respect to the research, authorship and publication of this article.

## Funding

The authors received no financial support for the research, authorship and publication of this article.

## Data Availability Statements

The datasets generated and/or analyzed during the current study are available from the corresponding author on reasonable request.

## Nomenclature

| | |
|---|---|
| $C$ | Constant |
| $D$ | Molecular diffusivity coefficient |
| $D_t$ | Turbulent molecular diffusivity coefficient |
| $E$ | Total energy (J) |
| $G_b$ | Generation of turbulence kinetic energy due to buoyancy |
| $G_k$ | Generation of turbulence kinetic energy due to the mean velocity gradients |
| $g$ | Gravity acceleration (m/s$^2$) |
| $h$ | Enthalpy (J) |
| $k$ | Turbulence kinetic energy (J) |
| $K_{eff}$ | Effective conductivity (W/mk) |
| $P$ | Static pressure (Pa) |
| $S$ | Source terms |
| $S_i$ | The contaminant generation rate |
| $T$ | Temperature (K) |
| $V$ | Velocity (m/s) |
| $\vec{v}$ | Velocity vector (m/s) |
| $Y_M$ | Contribution of the fluctuating dilatation |

**Greek Symbols**

| | |
|---|---|
| $\upsilon$ | Kinematic viscosity (m$^2$/s) |
| $\mu$ | Dynamic viscosity (kg/ms) |
| $\mu_{eff}$ | Turbulent viscosity coefficient (Pas) |
| $\mu_t$ | Turbulence viscosity (kg/ms) |
| $\rho$ | Fluid density (kg/m$^3$) |
| $\rho_0$ | Specified density of air(kg/m$^3$) |

| | |
|---|---|
| $\rho_\beta$ | Boussinesq density (kg/m$^3$) |
| $\bar{\bar{\tau}}$ | Stress tensor (Pa) |
| $\bar{\bar{\tau}}_{ef}$ | Deviatoric stress tensor (Pa) |
| $\beta$ | Thermal expansion coefficient (k$^{-1}$) |
| $\sigma_k$ | Turbulent Prandtl number for k |
| $\sigma_\varepsilon$ | Turbulent Prandtl number for ε |
| $\varepsilon$ | Rate of dissipation (m$^2$/s$^3$) |
| $\bar{Y}_i$ | Species concentration |

**Abbreviations**

| | |
|---|---|
| ACH | Air change rate per hour |
| ASHRAE | American society of heating, refrigerating and air-conditioning engineers |
| CFD | Computational fluid dynamic |
| HVAC | Heating, ventilation and air conditioning |
| IJV | Impinging jet ventilation |
| ISC | Iranian surgery clinic |
| LAF | Laminar airflow |
| OR | Operating room |
| PIV | Particle image velocimetry |
| RH | Relative humidity |
| SZ | Surgical zone |
| TAF | Turbulent airflow |

## References


[1] Hwang, R.L., Lin, T.P., Cheng, M.J., Chien, J.H., Patient thermal comfort requirement for hospital environments in Taiwan, *Building and Environment*, 42(8), 2007, 2980-2987.
[2] Khodakarami, J., Nasrollahi, N., Thermal comfort in hospitals - a literature review, *Renewable and Sustainable Energy Reviews*, 16(6), 2012, 4071-4077.
[3] Ding, L.C., Yau, Y.H., A study on the arrangement of air inlets in a class 7 clean room, *Building Services Engineering Research & Technology*, 36(3), 2015, 357-367.
[4] Lee, K.S., Zhang, T., Jiang, Z., Chen, Q., Comparison of airflow and contaminant distributions in rooms with traditional displacement ventilation and under-floor air distribution systems, *ASHRAE Transactions*, 115(2), 2009, 306-321.
[5] Wladyslaw, J.K., *Air treatment systems for controlling hospital acquired infections*, Immune Building Systems HPAC Engineering, New York, 2007.
[6] Memarzadeh, F., Jiang, Z., Effect of operation room geometry and ventilation system parameter variations on the protection of the surgical site, *IAQ*, 2004, 1-6.
[7] Cook, M., *The design quality manual: improving building performance*, John Wiley & Sons, 2008.
[8] McNeill, J., Hertzberg, J., Zhai, Z.J., Experimental investigation of operating room air distribution in a full-scale laboratory chamber using particle image velocimetry and flow visualization, *Flow Control, Measurement & Visualization*, 1, 2013, 24-32.
[9] Van Gaever, R., Jacobs, V.A., Diltoer, M., Peeters, L., Vanlanduit, S., Thermal comfort of the surgical staff in the operating room, *Building and Environment*, 81, 2014, 37-41.
[10] Ufat, H., Kaynakli, O., Yamankaradeniz, N., Yamankaradeniz, R., Three-dimensional air distribution analysis of different outflow typed operating rooms at different inlet velocities and room temperatures, *Advances in Mechanical Engineering*, 9(7), 2017, 1-12.
[11] Zhai, Z.J., Osborne, A.L., Simulation-based feasibility study of improved air conditioning systems for hospital operating room, *Frontiers of Architectural Research*, 2(4), 2013, 468-475.
[12] Pereira, M.L., Tribess, A., A review of air distribution patterns in surgery rooms under infection control focus, *Thermal Engineering*, 4, 2005, 113-121.
[13] Memarzadeh, F., Manning, A.P., Comparison of operating room ventilation systems in the protection of the surgical site, *ASHRAE Transactions*, 108(2), 2002, 3-15.
[14] Chow, T.T., Yang, X.Y., Performance of ventilation system in a non-standard operating room, *Building and Environment*, 38(12), 2003, 1401-1411.
[15] Chow, T.T., Yang, X.Y., Ventilation performance in the operating theatre against airborne infection: numerical study on an ultra-clean system, *Journal of Hospital Infection*, 59(2), 2005, 138-147.
[16] Chow, T.T., Lin, Z., Bai, W., The integrated effect of medical lamp position and diffuser discharge velocity on ultra-clean ventilation performance in an operating theatre, *Indoor and Built Environment*, 15(4), 2006, 315-331.
[17] Balaras, C.A., Dascalaki, E., Gaglia, A., HVAC and indoor thermal conditions in hospital operating rooms, *Energy and Buildings*, 39(4), 2007, 454-470.
[18] Rui, Z., Guangbei, T., Jihong, L., Study on biological contaminant control strategies under different ventilation models in hospital operating room, *Building and Environment*, 43(5), 2008, 793-803.
[19] Ho, S.H., Rosario, L., Rahman, M.M., Three-dimensional analysis for hospital operating room thermal comfort and contaminant removal, *Applied Thermal Engineering*, 29(10), 2009, 2080-2092.
[20] Liu, J., Wang, H., Wen, W., Numerical simulation on a horizontal airflow for airborne particles control in hospital operating room, *Building and Environment*, 44(11), 2009, 2284-2289.
[21] El Gharbi, N., Benzaoui, A., Khalil, E.E., Kameel, R., Analysis of indoor air quality in surgical operating rooms using experimental and numerical investigations, *Mechanics & Industry*, 13, 2012, 123-126.
[22] Yau, Y.H., Ding, L.C., A case study on the air distribution in an operating room at Sarawak general hospital heart centre (SGHHC) in Malaysia, Indoor and Built Environment, 23(8), 2014, 1129-1141.
[23] Kobayashi, T., Sugita, K., Umemiya, N., Kishimoto, T., Sandberg, M., Numerical investigation and accuracy verification of indoor environment for an impinging jet ventilated room using computational fluid dynamics, *Building and Environment*, 115, 2017, 251-268.
[24] Sadrizadeh, S., Afshari, A., Karimipanah, T., Håkansson, U., Nielsen, P.V., Numerical simulation of the impact of surgeon posture on airborne particle distribution in a turbulent mixing operating theatre, *Building and Environment*, 110, 2016, 140-147.
[25] Van Gaever, R., Jacobs, V.A., Diltoer, M., Peeters, L., Vanlanduit, S., Thermal comfort of the surgical staff in the operating room, *Building and Environment*, 81, 2014, 37-41.

[26] Loomans, M.G.L.C., de Visser, I.M., Loogman, J.G.H., Kort, H.S.M., Alternative ventilation system for operating theaters: Parameter study and full-scale assessment of the performance of a local ventilation system, *Building and Environment*, 102, 2016, 26-38.
[27] King, M.F., Noakes, C.J., Sleigh, P.A., Modeling environmental contamination in hospital single- and four-bed rooms, *Indoor Air*, 25(6), 2015, 694-707.
[28] Gronlund, C.J., Berrocal, V.J., Modeling and comparing central and room air conditioning ownership and cold-season in-home thermal comfort using the American Housing Survey, *Journal of Exposure Science & Environmental Epidemiology*, 30(5), 2020, 814–823.
[29] Figuerola-Tejerina, A., Hernández-Aceituno, A., Alemán-Vega, G., Orille-García, C., Ruiz-Álvarez, M., Sandoval-Insausti, H., Developing a faster way to identify biocontamination in the air of controlled environment rooms with HEPA filters: airborne particle counting, *Scientific Reports*, 10(1), 2020, 1-8.
[30] Ryan, R. M., Wilding, G. E., Wynn, R. J., Welliver, R. C., Holm, B. A., Leach, C. L., Effect of enhanced ultraviolet germicidal irradiation in the heating ventilation and air conditioning system on ventilator-associated pneumonia in a neonatal intensive care unit, *Journal of Perinatology*, 31(9), 2011, 607-614.
[31] *ASHRAE, ANSI Standard 170-2013 Ventilation of Health Care Facilities*, American Society of Heating, Refrigerating and Air-Conditioning Engineers, Inc, Atlanta, 2013.
[32] *ASHRAE, ANSI Standard 170-2008 Ventilation of Healthcare Facilities*, American Society of Heating, Refrigerating and Air-Conditioning Engineers, Inc, Atlanta, 2008.
[33] Ning, M., Mengjie, S., Mingyin, C., Dongmei, P., Shiming, D., Computational fluid dynamics (CFD) modelling of airflow field, mean age of air and $CO_2$ distributions inside a bedroom with different heights of conditioned air supply outlet, *Applied Energy*, 164, 2016, 906-915.
[34] Deng, H.Y., Feng, Z., Cao, S.J., Influence of air change rates on indoor $CO_2$ stratification in terms of Richardson number and vorticity, *Building and Environment*, 129, 2018, 74-84.
[35] Zheng, C., You, S., Zhang, H., Zheng, W., Zheng, X., Ye, T., Liu, Z., Comparison of air-conditioning systems with bottom-supply and side-supply modes in a typical office room, *Applied Energy*, 227, 2018, 304-311.
[36] Tung, Y.C., Shih, Y.C., Hu, S.C., Numerical study on the dispersion of airborne contaminants from an isolation room in the case of door opening, *Applied Thermal Engineering*, 29(8-9), 2009, 1544-1551.
[37] *ASHRAE, HVAC Design Manual for Hospitals and Clinics*, American Society of Heating, Refrigerating and Air-Conditioning Engineers, Inc, Atlanta, 2003.

## ORCID iD

Vahid Gholami Motlagh https://orcid.org/0000-0002-7273-667X
Mohammad Ahmadzadehtalatapeh https://orcid.org/0000-0002-9164-7592



**How to cite this article:** Gholami Motlagh V., Ahmadzadehtalatapeh M. Optimization of air distribution patterns by arrangements of air inlets and outlets: case study of an operating room, *J. Appl. Comput. Mech.*, 8(3), 2022, 809–830. https://doi.org/10.22055/JACM.2020.32443.2015